



Aalborg Universitet

AALBORG UNIVERSITY  
DENMARK

## Three-level (TL) based isolated DC/DC converters with improved performances

Liu, Dong

DOI (link to publication from Publisher):  
[10.5278/VBN.PHD.ENG.00043](https://doi.org/10.5278/VBN.PHD.ENG.00043)

Publication date:  
2018

Document Version  
Publisher's PDF, also known as Version of record

[Link to publication from Aalborg University](#)

Citation for published version (APA):

Liu, D. (2018). *Three-level (TL) based isolated DC/DC converters with improved performances*. Aalborg Universitetsforlag. <https://doi.org/10.5278/VBN.PHD.ENG.00043>

### General rights

Copyright and moral rights for the publications made accessible in the public portal are retained by the authors and/or other copyright owners and it is a condition of accessing publications that users recognise and abide by the legal requirements associated with these rights.

- Users may download and print one copy of any publication from the public portal for the purpose of private study or research.
- You may not further distribute the material or use it for any profit-making activity or commercial gain
- You may freely distribute the URL identifying the publication in the public portal -

### Take down policy

If you believe that this document breaches copyright please contact us at [vbn@aub.aau.dk](mailto:vbn@aub.aau.dk) providing details, and we will remove access to the work immediately and investigate your claim.

**THREE-LEVEL (TL) BASED  
ISOLATED DC/DC CONVERTERS  
WITH IMPROVED PERFORMANCES**

**BY  
DONG LIU**

DISSERTATION SUBMITTED 2018



**AALBORG UNIVERSITY**  
DENMARK



# **THREE-LEVEL (TL) BASED ISOLATED DC/DC CONVERTERS WITH IMPROVED PERFORMANCES**

by

DONG LIU



**AALBORG UNIVERSITY**  
DENMARK

Dissertation submitted 2018

Dissertation submitted: January 26, 2018

PhD supervisor: Prof. Zhe Chen  
Aalborg University

Assistant PhD supervisor: Assistant Prof. Fujin Deng  
Aalborg University

PhD committee: Professor Stig Munk-Nielsen (Chairman)  
Aalborg University

Professor Brad Lehman  
Northeastern University

Mauro Cappelli  
ENEA  
Frascati Res. Center

PhD Series: Faculty of Engineering and Science, Aalborg University

Department: Department of Energy Technology

ISSN (online): 2446-1636  
ISBN (online): 978-87-7210-141-5

Published by:  
Aalborg University Press  
Langagervej 2  
DK – 9220 Aalborg Ø  
Phone: +45 99407140  
aauf@forlag.aau.dk  
forlag.aau.dk

© Copyright: Dong Liu

Printed in Denmark by Rosendahls, 2018



## CV

Dong Liu (S'15) received the B.Eng. degree and M.Sc. degree in Electrical Engineering from South China University of Technology, Guangdong, China, in 2008 and 2011 respectively. He is currently working toward the Ph.D. degree in the Department of Energy Technology, Aalborg University, Denmark. From 2011 to 2014, he was a R&D Engineer in Emerson Network Power Co., Ltd., Shenzhen, China.

His main research interests include renewable energy technology, DC/DC converters, and multilevel converters.



# ENGLISH SUMMARY

AC grids are widely used nowadays for the electrical distribution system. However, the clear merits including no frequency stability, no reactive power, and simple system control of DC grids make it become the promising solution for the future electrical distribution system. In DC grids, DC/DC converters are one of most important composed components. Generally, increasing DC bus voltage is effectively way to decrease transmission power loss in DC grids. Three-level (TL) based isolated DC/DC converters (TL-IDCs) are one of most attractive choices for DC grids of DC bus with medium voltage because voltage stress of power switches is half of input voltage. Accordingly, this project mainly focuses on unidirectional TL-IDCs for DC loads such as data centre, electric vehicle, and so on.

The current research about TL-IDCs mainly includes following topics: 1) reducing switching noises; 2) increasing the converter's efficiency; and 3) increasing the converter's power density. However, only a few papers pay attentions on performances of TL-IDCs including input capacitor, power device, and transformer. Accordingly, this project investigates the control strategies to enhance the performances of input capacitor, power switch, and transformer in TL-IDCs.

For improving the input capacitor performance, this project proposes a zero-voltage switching (ZVS) control strategy including a periodically swapping modulation (PSM) strategy for four-switch half-bridge three-level (FS-HBTL) DC/DC converter to balance two input capacitors' currents, which would thus balance input capacitors' thermal stress and lifetime. Additionally, input-parallel output-parallel (IPOP) TL isolated DC/DC converters are proposed in this project for balancing and minimizing currents among input capacitors, which would thus reduce input capacitor's size or prolong input capacitor's lifetime.

For improving the power device performance, the proposed PSM strategy can be also utilized for TL-IDCs with asymmetrical control strategy to balance power devices' currents in, which would thus balance the power devices' thermal stress and power loss.

For improving the isolated transformer performance in full-bridge (FB) diode-clamped TL isolated DC/DC converter, this project proposes a new double phase-shift (DPS) control strategy to decrease voltage changes on the transformer by generating the multi-level voltage, which would thus decrease voltage change stress and voltage change rate ( $dv/dt$ ) on transformer.

Finally, simulation results and experimental results both verify proposed strategies and topology.





# DANSK RESUME

AC grids are widely used nowadays for the electrical distribution system. Men, de klare meriter, herunder ikke frekvensstabilitet, ingen reaktiv kraft, og enkel systemkontroll av DC grids gjør det til en lovende løsning for fremtidens elektriske distribusjonssystem. In DC grids, DC/DC converters are one of the most important composed components. Generally, increasing DC bus voltage is the effective way to reduce transmission power loss in DC grids. Three-level (TL) based DC/DC converters (TL-IDCs) are one of most attractive choices for DC grids or DC bus with medium voltage because voltage stress on power switches are half of input voltage. Følgelig, dette projekt fokuserer hovedsakelig på unidirectional TL-IDCs for DC-belastninger som datasenter, elektrisk kjøretøy, og så videre.

De huidige onderzoek over TL-IDC's omvat hoofdzakelijk volgende topics: 1) reducing switching noises; 2) increasing the converter's efficiency; and 3) increasing the converter's power density. Men, kun et par papirer betaler opmærksomheder på forestillinger eller TL-IDCs, inklusive input-kondensator, strømforsyning og transformer. Consequently, this project investigates the control strategies to enhance the performance of input capacitor, power switch, and transformer in TL-IDCs.

For at forbedre indgangskondensatorens ydeevne foreslår dette projekt en nulspændingsomskifter (ZVS) kontrolstrategi, herunder en periodisk swapping modulation (PSM) strategi for fire-switch halv-bridge tre-niveau (FS-HBTL) DC/DC konverter til balance to indgangskondensatorer 'strømme, hvilket således vil balancere indgangskondensatorernes termiske stress og levetid. Derudover foreslås input parallelle output parallelle (IPOP) TL isolerede DC/DC omformere i dette projekt for at afbalancere og minimere strømninger mellem indgangskondensatorer, hvilket således reducerer indgangskondensatorens størrelse eller forlænger indgangskondensatorens levetid.

For at forbedre effektenhedens ydeevne kan den foreslåede PSM-strategi udnyttes til TL-IDC'er med asymmetrisk kontrolstrategi for at afbalancere strømforsyningernes strømme  $i$ , hvilket således vil balancere strømforsyningenshedernes termiske spænding og effekttab.

For at forbedre den isolerede transformator ydeevne i fuldbro (FB) diode-clampede TL-isolerede DC/DC-omformer, foreslår dette projekt en ny styringsstrategi med dobbelt faseforskydning (DPS) for at reducere spændingsændringer på transformeren ved at generere multiniveaueet spænding, hvilket således ville mindske spændingsændringsspændingen og spændingsændringshastigheden ( $dv/dt$ ) på transformeren.

Endelig kontrollerer simuleringsresultater og eksperimentelle resultater både foreslåede strategier og topologi.

# ACKNOWLEDGEMENTS

The Ph.D. study, entitled ‘Three-level (TL) based isolated DC/DC converters with improved performances’, is from December 2014 until January 2018 under the supervision of Prof. Zhe Chen at Energy Technology Department, Aalborg University (AAU), Denmark. I would deeply thank China Scholarship Council (CSC) for supporting my financial cost in my Ph.D. study.

First, I would express my deeply appreciation to my supervisor Prof. Zhe Chen. I appreciate his ideas, guidance, encouragements, and time to make my Ph.D. research stimulating and smoothly. Additionally, his high research enthusiasm encourages and motivates me a lot. His wise advices both on my research and career are priceless.

My sincerely thanks are also given to my co-supervisor, Assistance Prof. Fujin Deng, for his constructive mentor, professional suggestions, patient explanations, and continuous encouragements.

High tribute shall be paid to Prof. Fred Lee, Prof. Qiang Li, colleagues, and friends for their kindness and helps during my studying in Center for Power Electronics Systems (CPES), Virginia Tech University, where I benefited a lot from discussion with them.

I would sincerely appreciate my committee members, Prof. Stig Munk-Nielsen, Prof. Brad Lehman, and Prof. Mauro Cappelli. Thanks a lot for paying your time to reading my thesis and coming to attend my committee members.

The members in my research group have made immense contributions to my personal and research time at Aalborg University. This research group has very good collaborations and discussions between each other. I would like to appreciate all my group members, Rui Hu, Pengfei Li, Yanbo Wang, Qing Zeng, Jiakun, Fang, Chi Su, Nuri Gökmen, Weihao Hu, Baohua Zhang, Chao Wang, Yanjun Tian, Rongwu Zhu, and numerous guest researchers and students who have come visiting our lab for their friendship and support, which creates a joyful and enthusiastic research and living environment for me. I am so grateful for spending pleasant time with them.

I am also grateful to have the colleagues in other search groups in Aalborg University, Baoze Wei, Zhen Xin, Yajuan Guan, and all, for their helpful advices and support.

I want to send my gratitude to all staffs and friends in Department of Energy Technology for their help during my research. My research time at Aalborg University was very enjoyable because of many colleagues, friends and groups that became a part of my life.

Finally, I would provide my deepest thanks to my wife, Dr. Ying Li, my brother, my parents, my parents-in-law, and all my families for their continuous encouragements, important supports, and endless love.

Dong Liu

刘栋

Aalborg University  
Aalborg, Denmark

08-01-2018

# TABLE OF CONTENTS

<b>Chapter 1. Introduction</b>	<b>19</b>
1.1. Background and motivations.....	19
1.2. Literature review .....	21
1.3. Research objectives.....	23
1.3.1. Input capacitor performance.....	23
1.3.2. Power device performance .....	25
1.3.3. Transformer performance .....	26
1.4. Thesis outline .....	27
1.5. List of publications.....	28
<b>Chapter 2. Improving input capacitor performances</b>	<b>31</b>
2.1. ZVS control strategy with balanced input capacitor current .....	31
2.1.1. Input capacitor current imbalance issue .....	31
2.1.2. ZVS control strategy .....	34
2.1.3. PSM strategy .....	34
2.1.4. Simulation and experimental verification .....	38
2.2. IPOP TL isolated DC/DC converters .....	43
2.2.1. Circuit structure.....	43
2.2.2. Working principle .....	43
2.2.3. Currents on input capacitors.....	46
2.2.4. Simulation and experimental verification .....	48
2.3. Summary .....	51
<b>Chapter 3. Improving power device performance</b>	<b>52</b>
3.1. Power device current imbalance issue.....	52
3.2. Power devices' currents under PSM strategy.....	54
3.3. Simulation and experimental verification .....	57
3.4. Summary .....	61
<b>Chapter 4. Improving transformer performance</b>	<b>62</b>
4.1. Voltage changes on transformer under conventional control strategy .....	62
4.2. Proposed DPS control strategy.....	63

4.3. Simulation verification.....	66
4.4. Summary .....	67
<b>Chapter 5. Conclusions and future works</b>	<b>68</b>
<b>Literature list</b>	<b>70</b>

# LIST OF ACRONYMS

DPS	Double phase-shift
FB	Full-bridge
FS-HBTL	Four-switch half-bridge three-level
HBTL	Half-bridge three-level
IPOP	Input-parallel output-parallel
IDCs	Isolated DC/DC converters
PSM	Periodically swapping modulation
TL	Three-level
TL-IDCs	Three-level based isolated DC/DC converters
ZVS	Zero-voltage switching



# TABLE OF FIGURES

Figure 1-1 General DC grids architecture layout. ....	19
Figure 1-2 Three basic kinds. (a) Two-level isolated DC/DC converter. (b) TL isolated DC/DC converter. (c) MMC. ....	21
Figure 1-3 Basic topologies of TL IDCs. (a) Diode clamped HBTL isolated DC/DC converter [62]. (b) Diode clamped HBTL isolated DC/DC converter with flying capacitor [63]. (c) FS-HBTL isolated DC/DC converter [75]. ....	22
Figure 1-4 TL hybrid isolated DC/DC converter [92]. ....	24
Figure 1-5 FB TL-based isolated DC/DC converter with voltage auto-balance ability of input capacitors [93]. ....	24
Figure 1-6 (a) Flying capacitor TL isolated DC/DC converter. (b) HBTL isolated DC/DC converter including two transformers. (c) Dual HBTL isolated DC/DC converter. ....	26
Figure 1-7 FB TL isolated DC/DC converter with flying capacitors. ....	27
Figure 1-8 Improved FB TL isolated DC/DC converter [99]. ....	27
Figure 2-1 (a) Circuit structure. (b) Conventional control strategy [75]. ....	32
Figure 2-2 Proposed ZVS strategy. (a) Operation mode I. (b) Operation mode II. ...	34
Figure 2-3 Proposed PSM strategy [100]. ....	35
Figure 2-4 Calculated RMS value of $i_{c1}$ , $i_{c2}$ ( $V_o = 50V$ ). ....	37
Figure 2-5 Calculated deviations between RMS value of $i_{c1}$ , $i_{c2}$ under the conventional control strategy ( $V_o = 50V$ ). ....	38
Figure 2-6 Simulation results ( $V_{in} = 550 V$ , $V_o = 50 V$ , $P_o = 1 kW$ ). (a) Conventional strategy. (b) Proposed strategy. ....	38
Figure 2-7 Hardware of established prototype. ....	39
Figure 2-8 Control block of proposed PSM strategy. ....	39
Figure 2-9 ZVS performance of $S_1$ ( $V_{in} = 550 V$ , $V_o = 50 V$ ). (a) $P_o = 500 W$ . (b) $P_o = 1 kW$ . ....	40
Figure 2-10 ZVS performance of $S_3$ ( $V_{in} = 550 V$ , $V_o = 50 V$ ). (a) $P_o = 500 W$ . (b) $P_o = 1 kW$ . ....	40
Figure 2-11 Experimental results of $V_{in}$ , $V_o$ , $i_o$ , and $i_p$ ( $V_{in} = 550 V$ , $V_o = 50V$ , $P_o = 1 kW$ ) [100]. (a) Conventional strategy. (b) Proposed strategy. ....	41
Figure 2-12 Experimental results of $V_1$ , $V_2$ , $V_{cb}$ , and $i_{c2}$ ( $V_{in} = 550 V$ , $V_o = 50V$ , $P_o = 1 kW$ ) [100]. (a) Conventional strategy. (b) Proposed strategy. ....	41
Figure 2-13 Experimental results of $V_{ab}$ , $i_{c1}$ , and $i_{c2}$ ( $V_{in} = 550 V$ , $V_o = 50V$ , $P_o = 1 kW$ ) [100]. (a) Conventional strategy. (b) Proposed strategy. ....	41
Figure 2-14 Experimental RMS value of $i_{c1}$ , $i_{c2}$ ( $V_o = 50 V$ , $P_o = 1 kW$ ). ....	42
Figure 2-15 Dynamic performances under load changes (1 kW to 500 W to 1 kW) ( $V_{in} = 550 V$ $V_o = 50 V$ ). ....	42
Figure 2-16 Experimental efficiency results ( $V_o = 50 V$ ). ....	42
Figure 2-17 Circuit structure. ....	43
Figure 2-18 (a) Without interleaving control strategy. (b) With interleaving control strategy. [101] ....	44

Figure 2-19 Equivalent circuits with interleaving control strategy [101]. (a) $[t_0-t_1]$ . (b) $[t_1-t_2]$ . (c) $[t_2-t_3]$ . (d) $[t_3-t_4]$ . (e) $[t_4-t_5]$ . (f) $[t_5-t_6]$ . (g) $[t_6-t_7]$ . .....	45
Figure 2-20 Calculation results about RMS value of $i_{c1}$ , $i_{c2}$ ( $V_o = 50$ V). .....	48
Figure 2-21 Simulation results ( $V_{in} = 550$ V, $V_o = 50$ V, and $P_o = 1$ kW). (a) Without interleaving control strategy. (b) With interleaving control strategy. [101].....	48
Figure 2-22 Hardware of established prototype. ....	49
Figure 2-23 Experimental results of $V_{in}$ , $V_o$ , $i_{p1}$ , and $i_{p2}$ under 500 W ( $V_{in} = 550$ V, $V_o = 50$ V) [101]. (a) Without interleaving control strategy. (b) With interleaving control strategy.....	49
Figure 2-24 Experimental results of $i_{c1}$ , $i_{c2}$ , $V_{ab}$ , and $V_{cd}$ under 500 W ( $V_{in} = 550$ V, $V_o = 50$ V) [101]. (a) Without interleaving control strategy. (b) With interleaving control strategy.....	50
Figure 2-25 Experimental results of $V_{in}$ , $V_o$ , $i_{p1}$ , and $i_{p2}$ under 1 kW ( $V_{in} = 550$ V, $V_o = 50$ V) [101]. (a) Without interleaving control strategy. (b) With interleaving control strategy.....	50
Figure 2-26 Experimental results of $i_{c1}$ , $i_{c2}$ , $V_{ab}$ , and $V_{cd}$ under 1 kW ( $V_{in} = 550$ V, $V_o = 50$ V) [101]. (a) Without interleaving control strategy. (b) With interleaving control strategy.....	50
Figure 2-27 RMS value of $i_{c1}$ and $i_{c2}$ ( $V_o = 50$ V and $P_o = 1$ kW).....	51
Figure 3-1 (a) Circuit Structure. (b) Asymmetrical modulation strategy [75]. .....	53
Figure 3-2 Currents on power devices under proposed PSM strategy. ....	54
Figure 3-3 Equivalent circuits [102]. (a) [before $t_2$ ]. (b) $[t_2 - t_3]$ . (c) $[t_3 - t_5]$ . (d) $[t_5 - t_6]$ . (e) $[t_6 - t_7]$ . (f) $[t_7 - t_8]$ . (g) $[t_8 - t_9]$ . (h) $[t_9 - t_{10}]$ . (i) $[t_{10} - t_{12}]$ . (j) $[t_{12} - t_{13}]$ . (k) $[t_{13} - t_{14}]$ . (l) $[t_{14} - t_{15}]$ . (m) $[t_{15} - t_{16}]$ . .....	56
Figure 3-4 Simulation results ( $V_{in} = 4$ kV, $V_o = 400$ V, $i_o = 100$ A). (a) Asymmetrical modulation strategy. (b) Proposed strategy. ....	58
Figure 3-5 Experimental results of $V_{ab}$ , $V_o$ , $i_o$ , and $i_p$ ( $V_{in} = 550$ V, $V_o = 50$ V, $P_o = 1$ kW) [102]. (a) Asymmetrical modulation strategy. (b) Proposed strategy. ....	59
Figure 3-6 Experimental results of $i_1$ , $i_2$ , $i_3$ , and $i_4$ ( $V_{in} = 550$ V, $V_o = 50$ V, $P_o = 500$ W) [102]. (a) Asymmetrical modulation strategy. (b) Proposed strategy. ....	60
Figure 3-7 Experimental results of $i_1$ , $i_2$ , $i_3$ , and $i_4$ ( $V_{in} = 550$ V, $V_o = 50$ V, $P_o = 1$ kW) [102]. (a) Asymmetrical modulation strategy. (b) Proposed strategy. ....	60
Figure 3-8 Experimental RMS value of $i_1$ , $i_2$ , $i_3$ , and $i_4$ ( $V_o = 50$ V, $P_o = 1$ kW).....	61
Figure 3-9 Comparison results about power devices' thermal stresses ( $V_{in} = 550$ V, $V_o = 50$ V, $P_o = 1$ kW) [102]. (a) Asymmetrical modulation strategy. (b) Proposed strategy.....	61
Figure 4-1 Circuit structure. ....	62
Figure 4-2 Chopping plus phase shift (CPS) control [97]. (a) Three-level mode. (b) Two-level mode. ....	63
Figure 4-3 Double phase-shift (DPS) control [98]. (a) Three-level mode. (b) Two-level mode. ....	63
Figure 4-4 Proposed strategy (Three level mode). ....	64
Figure 4-5 Equivalent circuits [103]. (a) $[t_0-t_1]$ . (b) $[t_1-t_2]$ . (c) $[t_2-t_3]$ . (d) $[t_3-t_4]$ . (e) $[t_4-t_5]$ . (f) $[t_5-t_6]$ . (g) $[t_6-t_7]$ . (h) $[t_7-t_8]$ . (i) $[t_8-t_9]$ . (j) $[t_9-t_{10}]$ . (k) $[t_{10}-t_{11}]$ . .....	65

Figure 4-6 Simulation results under proposed DPS strategy..... 66  
Figure 4-7 Comparison results. (a) Conventional strategies. (b) Proposed strategy. 67

# TABLE OF TABLES

Tabel 1-1 Comparison results about three basic kinds of converters .....	21
Tabel 2-1 Calculation formulas about RMS value of $i_{c1}$ , $i_{c2}$ .....	37
Tabel 2-2 Parameters of simulation model and experimental prototype .....	39
Tabel 2-3 Calculation formulas about RMS value of $i_{c1}$ , $i_{c2}$ .....	47
Tabel 2-4 Parameters in simulation and experiments.....	49
Tabel 3-1 Calculation formulas about RMS value of $i_1 \sim i_4$ .....	57
Tabel 3-2 Parameters of established simulation model .....	57
Tabel 3-3 Parameters of established prototype .....	59
Tabel 4-1 Parameters of established simulation model .....	66



# CHAPTER 1. INTRODUCTION

## 1.1. BACKGROUND AND MOTIVATIONS

The clear advantages of DC grids such as no frequency stability, no reactive power, and simple system control make DC grids become promising choice for future smart power distribution system [1-8] in comparison with AC grids [9-11]. Additionally, DC-based data centres are being developed quickly nowadays [12], [13]. The liberalization of energy market also drive the requirement for developing DC grids technology, which has resulted in installations of large scale clean energy as fuel cells, wind power, solar power, and so on. Moreover, DC interfaces have already been widely employed for end-use consumers at various applications.

The general layout of DC grids is shown as Fig. 1-1.

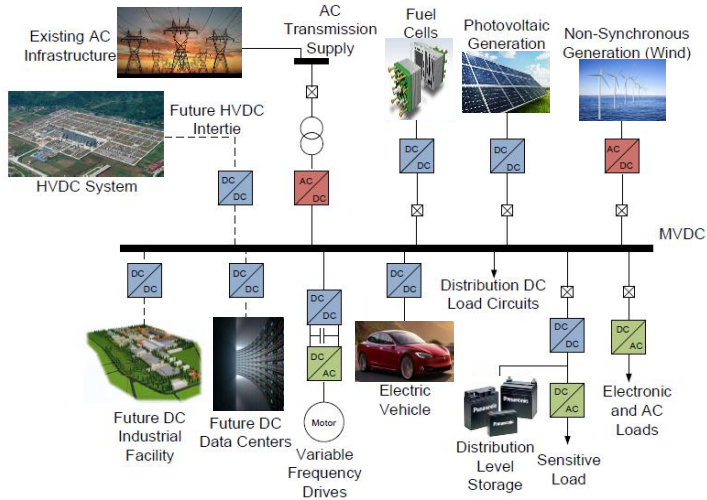
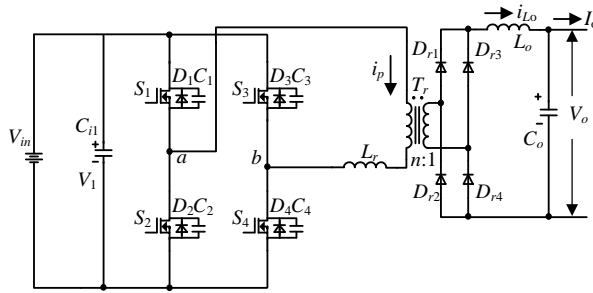


Figure 1-1 General DC grids architecture layout.

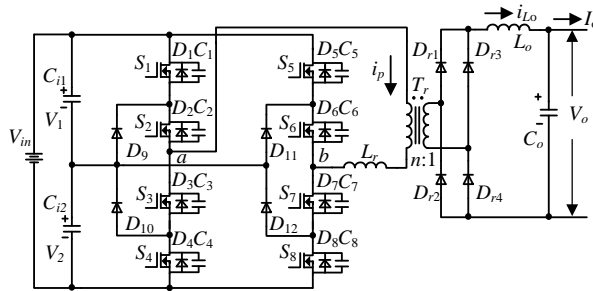
Generally, performances of DC grids are highly determined by DC/DC converters since voltage grade conversion and power transmission in DC grids are highly depended on these DC/DC converters [14-16]. Therefore, DC grids desires for DC/DC converters with high performances. Accordingly, this Ph.D. project aims at improving performances of DC/DC converters in aspect of the converter's reliability.

So far, literatures proposes many DC/DC converters which are mainly categorized into two types named non-isolated DC/DC converters [17-26] and isolated DC/DC converters (IDCs) [27-37]. Non-isolated converters cannot obtain galvanic isolation and high voltage conversion gain. Contrarily, IDCs can obtain high voltage gain, galvanic isolation due to isolated transformer and thus improve system safety. Accordingly, this project focuses on IDCs. Many IDCs have been proposed categorized into three kinds named two-level based IDCs, three-level based isolated DC/DC converters (TL-IDCs), and modular multilevel isolated DC/DC converters (MMC) [38] as presented in Fig. 1-2.

The minimal numbers of power switches are needed in two-level based IDCs [39-47] among these three kinds of converters. However, power switches' voltage stress of two-level based IDCs is full input voltage, which would thus lead high  $dv/dt$  on transformer, high switching loss, large electromagnetic interference (EMI) [48], [49]. MMC [50-57] differentiate themselves from other converters with good power quality, low voltage stress of power devices, and small EMI. However, MMC needs more power switches and voltage transducers, and would thus lead to increasing cost and complex control algorithm (such as voltage balancing control of capacitor) [59-62]. TL-IDCs [62-69] have merits of lower switch voltage stress, smaller output filter size, and lower EMI when comparing with two-level based IDCs. Comparing with MMC, TL-IDCs have advantages of fewer circuit components, lower cost, and easier control algorithm.



(a)



(b)

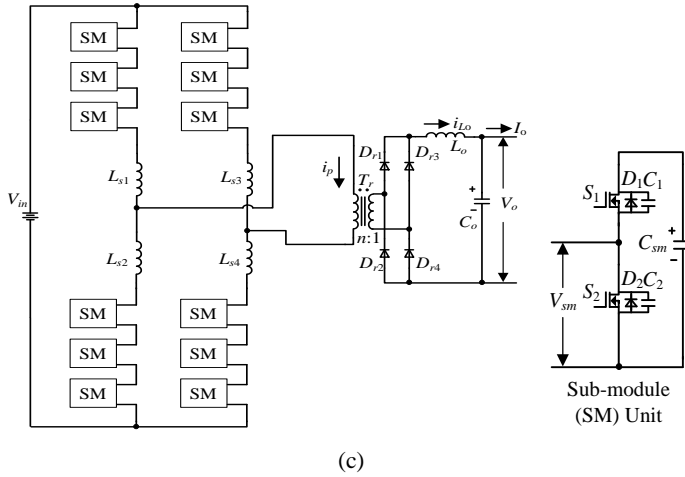


Figure 1-2 Three basic kinds. (a) Two-level isolated DC/DC converter. (b) TL isolated DC/DC converter. (c) MMC.

Comparison results between three basic kinds of DC/DC isolated converters are listed in Table 1-1. This Ph.D. project focuses on investigating unidirectional TL-IDCs' for DC loads such as data centre, electric vehicle in DC grids.

Table 1-1 Comparison results about three basic kinds of converters

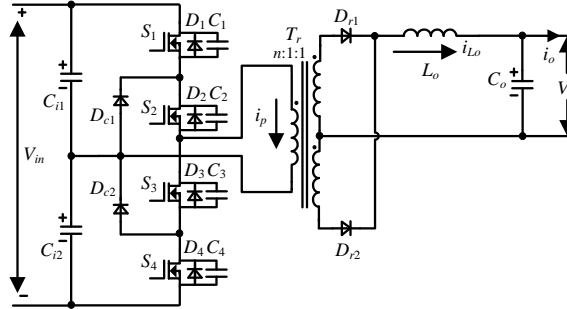
Converter Topology	Voltage of Switches	Voltage Balance Control Complexity	Cost
Two-level based IDCs	input voltage	no	low
TL-IDCs	half input voltage	easy	medium
MMC	less than or equal half input voltage based on the number of modules	complex	high

## 1.2. LITERATURE REVIEW

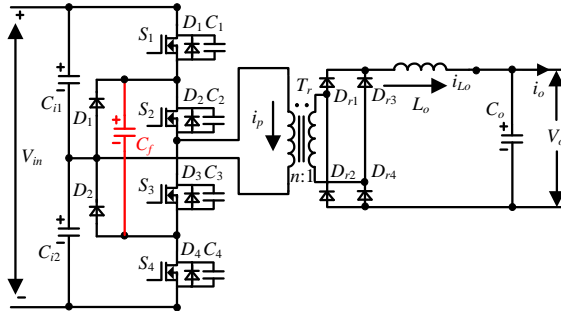
In 1992, a novel half-bridge TL (HBTL) isolated DC/DC converter presented in Fig. 1-3(a) was first proposed [62] to reduce power devices' voltage stress. Due to TL structure, power devices' voltage stress is decreased to be half of input voltage, which would make power devices with low-voltage-rated applicable for TL-IDCs. Therefore, TL-IDCs can be utilized in DC grids with DC bus of medium voltage.



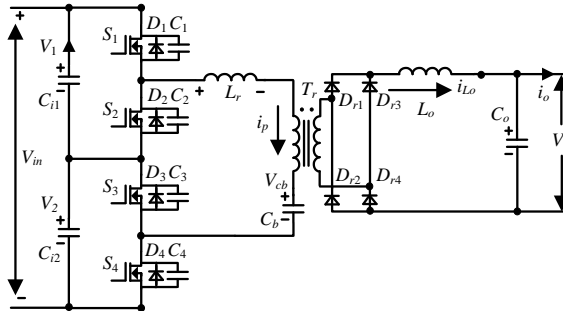
Besides HBTL isolated DC/DC converter in [62], there are also other basic topologies of TL-IDCs presented in Fig. 1-3.



(a)



(b)



(c)

Figure 1-3 Basic topologies of TL IDCs. (a) Diode clamped HBTL isolated DC/DC converter [62]. (b) Diode clamped HBTL isolated DC/DC converter with flying capacitor [63]. (c) FS-HBTL isolated DC/DC converter [75].

A HBTL isolated DC/DC converter including an added flying capacitor presented in Fig. 1-3 (b) was proposed in [63], which makes phase-shift control applicable. Reference [75] proposed a FS-HBTL isolated DC/DC as shown in Fig. 1-3 (c).

Comparing with conventional diode clamped HBTL IDCs [62], [63], FS-HBTL DC/DC converter has less components due to removing two clamping diodes.

So far, many studies have been done based on these basic topologies of TL-IDCs [70-97]. Based on investigation of these studies, there are mainly following three research topics:

- Expanding load range of soft switching achievement of TL-IDCs [70-74];
- Simplifying the circuit structure of TL-IDCs [75-80];
- Reducing the circulating current of TL-IDCs [83-88].

### 1.3. RESEARCH OBJECTIVES

Based on the above literature reviews, former studies about TL-IDCs mainly pay attention on aspects of reducing switching noises, increasing efficiency, and improving power density. However, only a few papers discuss about the reliability performances of TL-IDCs. Therefore, this Ph.D. project aims to investigate TL-IDCs' reliability to improve performances of TL-IDCs including input capacitor, power device, and transformer performance.

#### 1.3.1. INPUT CAPACITOR PERFORMANCE

Capacitor is one of most important components in terms of failure rate in practical working operations of power electronic systems [89], [90]. Many working conditions (e.g. temperature, humidity, current, voltage) play important roles in the reliability of capacitors. For the power electronics field, the rating voltage and current on the capacitor are fundamental factors for selecting the capacitor. The universal methods in the power electronics field to improve the capacitor reliability are: 1) reducing capacitor's voltage stress; 2) reducing capacitor's current. Because more than one input capacitor is utilized in TL-IDCs, many studies pay attentions on how to balance input capacitors' voltages. For instance, a voltage balancing control strategy was proposed in [91] to balance input capacitors' voltages in FS-HBTL isolated DC/DC converter presented in Fig. 1-3(c). Reference [92] proposed a TL hybrid isolated DC/DC converter with balanced input capacitors' voltage, whose circuit structure is presented in Fig. 1-4. Additionally, a FB TL-based isolated DC/DC converter was proposed in [93] as presented in Fig. 1-5, which has voltage auto-balance ability of input capacitors.

However, few papers investigate input capacitors' currents of TL-IDCs. Normally, capacitor temperature is mainly decided by capacitor current and ambient temperature around capacitor. More significantly, capacitor temperature would make a crucial influence on the capacitor's lifetime. Accordingly, this project focuses on

reducing and balancing input capacitors' currents of TL-IDCs, which can thus improve input capacitor reliability by reducing input capacitors' thermal stress and balancing input capacitors' lifetime.

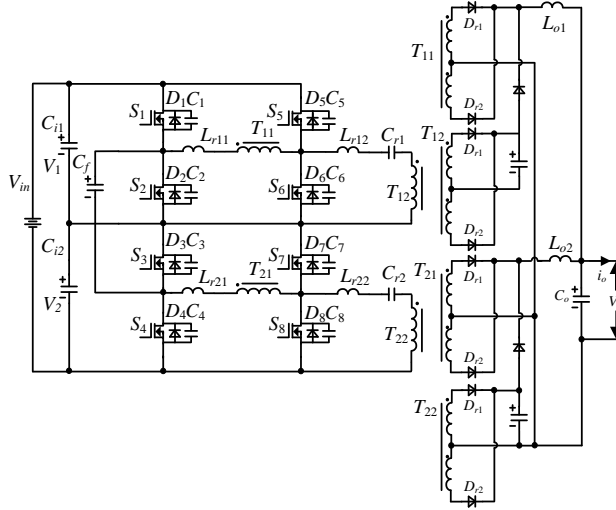


Figure 1-4 TL hybrid isolated DC/DC converter [92].

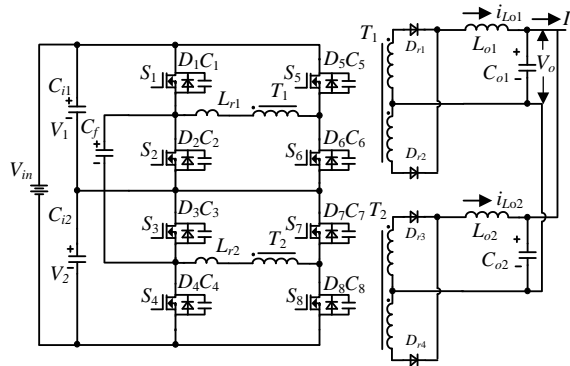


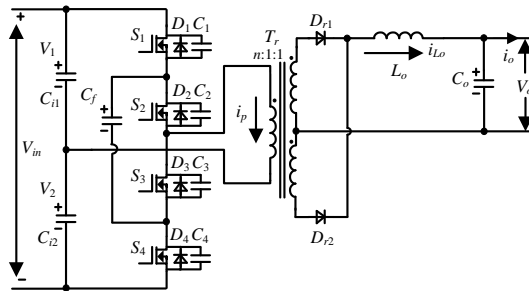
Figure 1-5 FB TL-based isolated DC/DC converter with voltage auto-balance ability of input capacitors [93].

A ZVS control strategy including a periodically swapping modulation (PSM) strategy is proposed in this project to balance input capacitors' currents for FS-HBTL isolated DC/DC converter, which can thus balance input capacitors' thermal stress and lifetime. Additionally, IPOP TL IDCs are proposed in this project to reduce and balance input capacitors' currents, which can thus prolong and balance input capacitors' lifetime.

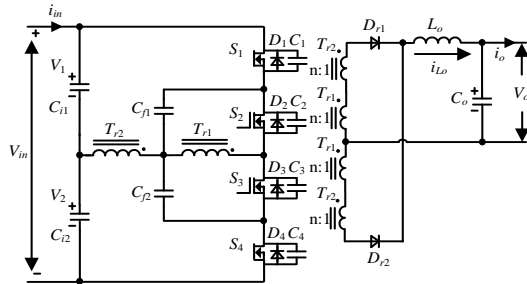
### 1.3.2. POWER DEVICE PERFORMANCE

The power device is another one of most significant components in power electronic systems because power generation and output/input voltage (or output/input current) are controlled by adjusting power devices' switching patterns. In addition, the cost of power devices normally occupies the dominant proportion in whole cost of power converter. Therefore, improving the reliability of power devices is significantly meaningful for enhancing the performances of converter. Normally, the temperature of power device is one of most significant parameters to judge whether the power switch operates reliably. Therefore, the thermal behaviors of power devices are quiet related to whole power electronic system's reliability performance.

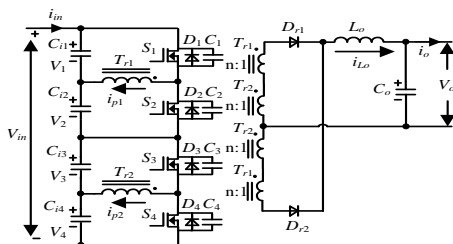
Generally, current through the power device is one of key factors that decides power device's power loss and thermal behavior. Asymmetrical modulation strategy is one of widely used modulation strategies for TL-IDCs [75], [94-96] as presented in Fig. 1-3(c) and Fig. 1-6.



(a)



(b)



(c)

Figure 1-6 (a) Flying capacitor TL isolated DC/DC converter. (b) HBTL isolated DC/DC converter including two transformers. (c) Dual HBTL isolated DC/DC converter.

Reference [94] proposed a flying capacitor based TL isolated DC/DC converter featuring with simple structure. Reference [95] proposed a TL isolated DC/DC converter including two transformers to reduce transformer windings' current stresses. Reference [96] proposed a TL isolated DC/DC converter including two transformers and two half-bridge structures. Additionally, reference [75] proposed a FS-HBTL isolated DC/DC converter, which has less circuit components comparing with diode-clamped TL isolated DC/DC converter. But, there exists one significant issue caused by asymmetrical modulation strategy in these TL-IDCs [75], [94-96] that primary power devices' currents are imbalanced, which would thus lead power devices' power loss and thermal stress imbalance. Accordingly, the proposed PSM strategy are utilized for these TL-IDCs to balance primary power devices' currents, which would thus improve converter's reliability performance by balancing power devices' power loss and thermal stress.

### 1.3.3. TRANSFORMER PERFORMANCE

The transformer is also one of significant components in isolated power converters because the transformer not only can provide high voltage conversion gain but also can isolate the electronic connection from primary to secondary side. Accordingly, improving the performance of transformer is meaningful for enhancing the performances of isolated converters. Normally,  $dv/dt$  is one of important factors which can make influence on the transformer of TL-IDCs. Accordingly, transformer's reliability can be improved by reducing  $dv/dt$  and voltage stress on transformer, which is helpful for improving converter's electromagnetic interference (EMI).

Chopping plus phase shift (CPS) and DPS control were proposed in [97] and [98] respectively for FB diode-clamped TL isolated DC/DC converter presented in Figure 1-7. However, high voltage change on transformer is caused by these control strategies, which would thus lead high  $dv/dt$  and electromagnetic interference (EMI). Therefore, a FB TL isolated DC/DC, as presented in Fig. 1-8, with a passive filter and a corresponding control strategy was proposed in [99], which can not only

decrease  $dv/dt$  but also balance input capacitors' voltages. But, added passive filter decreases converter's efficiency and voltage conversion gain. Therefore, this project proposes a new DPS control strategy for FB diode-clamped TL isolated DC/DC converter, which can decrease  $dv/dt$  and voltage stress on transformer.

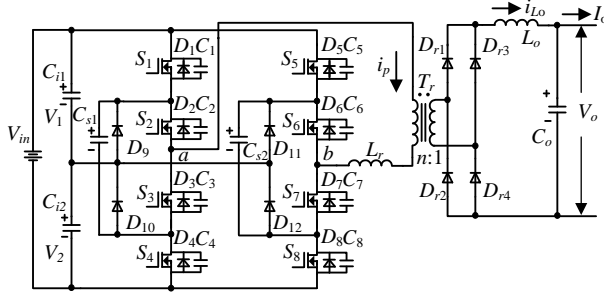


Figure 1-7 FB TL isolated DC/DC converter with flying capacitors.

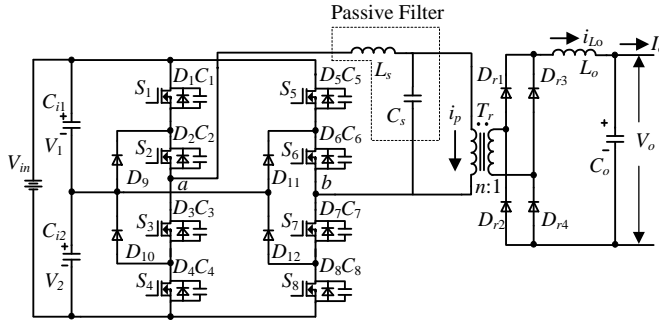


Figure 1-8 Improved FB TL isolated DC/DC converter [99].

## 1.4. THESIS OUTLINE

The organization about this thesis is introduced as follows.

**Chapter 2** introduce a ZVS strategy including a PSM strategy for FS-HBTL isolated DC/DC converter to balance two input capacitors' currents, which can thus balance input capacitors' thermal stress and lifetime. In addition, this project proposes IPOP TL IDCs for balancing and minimizing input capacitors' currents, which would thus prolong capacitors' lifetime or reduce capacitors' size. Published papers related to this chapter are J1, J2, C2, and C3.

**Chapter 3** illustrates that the proposed PSM strategy is utilized for TL-IDCs with asymmetrical modulation strategy. There exists power devices' current imbalance issue in TL-IDCs with asymmetrical modulation strategy, which would lead

unbalanced power loss and thermal stress of power devices. Accordingly, the proposed PSM strategy is utilized for these TL-IDCs to eliminate such current imbalance. Through using proposed strategy, power devices' power loss and thermal stress would be balanced, which would thus increase the converter's reliability. Published paper related to this chapter is J3.

**Chapter 4** introduces a new DPS control strategy for FB diode-clamped TL DC/DC converter. Because conventional control strategies causes the high  $dv/dt$  on isolated transformer, a new DPS strategy is proposed in this project to decrease  $dv/dt$  on transformer through generating multi-level voltage. Therefore, the proposed control strategy would decrease  $dv/dt$  and stress on transformer and is helpful for converter's EMI. Published paper related to this chapter is C1.

**Chapter 5** concludes the works of this thesis and introduces future works.

## 1.5. LIST OF PUBLICATIONS

A list of publications is given below. There are three published journal papers and three published conference papers related to this thesis. Three journal papers are marked as J1 ~ J3 and three conference papers are marked as C1 ~ C3.

Journal papers:

- J1. **D. Liu**, F. Deng, Z. Gong, and Z. Chen, "Input-parallel output-parallel (IPOP) three-level (TL) DC/DC converters with interleaving control strategy for minimizing and balancing capacitor ripple currents," in *IEEE Journal of Emerging and Selected Topics in Power Electronics*, vol. 5, no. 3, pp. 1122-1132, Sep. 2017.
- J2. **D. Liu**, F. Deng, Q. Zhang, and Z. Chen, "Zero-voltage switching PWM strategy based capacitor current-balancing control for half-bridge three-level DC/DC converter", in *IEEE Transactions on Power Electronics*, vol. 33, no. 1, pp. 357-369, Jan. 2018.
- J3. **D. Liu**, F. Deng, Q. Zhang, and Z. Chen, "Periodically swapping modulation (PSM) strategy for three-level (TL) DC/DC converters with balanced switch currents", in *IEEE Transactions on Industrial Electronics*, vol. 65, no. 1, pp. 412-423, Jan. 2018.

Conference papers:

- C1. **D.Liu**, F. Deng, Z. Gong, and Z, Chen, “A double phase-shift control strategy for a full-bridge three-level DC/DC converter”, in 42nd Annual Conference of the IEEE Industrial Electronics Society (IECON), Florence, Italy, 2016.
- C2. **D.Liu**, F. Deng, Q. Zhang, Z. Gong, and Z, Chen, “Input-parallel output-parallel (IPOP) three-level (TL) DC/DC converters with minimized capacitor ripple currents”, in IEEE Annual Southern Power Electronics Conference (SPEC), Auckland, New Zealand, 2016.
- C3. **D.Liu**, F. Deng, and Z, Chen, “A ZVS PWM control strategy with balanced capacitor current for half-bridge three-level DC/DC converter”, in 2017 IEEE Applied Power Electronics Conference and Exposition (APEC), Tampa, USA, 2017.





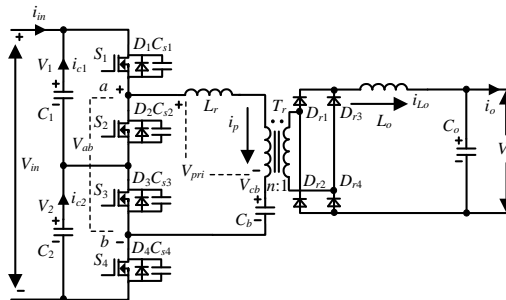
# CHAPTER 2. IMPROVING INPUT CAPACITOR PERFORMANCES

This chapter aims at improving input capacitor performances of TL-IDCs. Firstly, a ZVS control strategy including a PSM strategy for FS-HBTL isolated DC/DC converter is proposed to balance input capacitors' currents. Additionally, IPOP TL IDCs are proposed to balance and decrease input capacitors' currents. Finally, summary is given.

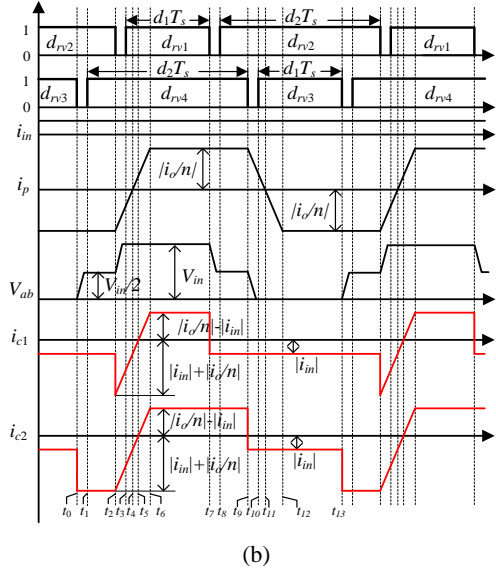
## 2.1. ZVS CONTROL STRATEGY WITH BALANCED INPUT CAPACITOR CURRENT

### 2.1.1. INPUT CAPACITOR CURRENT IMBALANCE ISSUE

Figure 2-1(a) presents the FS-HBTL isolated DC/DC converter [75]. In Figure 2-1(a),  $V_{in}$  is input voltage;  $C_1$  and  $C_2$  are two input capacitors to split  $V_{in}$  into two voltages  $V_1$  and  $V_2$ ;  $S_1 - S_4$  are power switches;  $D_1 - D_4$  are power diodes;  $T_r$  is isolated transformer;  $L_r$  is leakage inductor of  $T_r$ ;  $C_{s1} - C_{s4}$  are parasitic capacitors of  $S_1 - S_4$ ;  $C_b$  is DC-blocking capacitor;  $D_{r1} - D_{r4}$  are four rectifier diodes;  $L_o$  is filter inductor; and  $C_o$  is filter capacitor. Additionally, the input current is  $i_i$ ; currents flowing through  $C_1$  and  $C_2$  are  $i_{c1}$  and  $i_{c2}$ ; primary voltage and current on  $T_r$  are  $V_{pri}$  and  $i_p$ ; the current through  $L_o$  is  $i_{Lo}$ ; the voltage on  $C_b$  is  $V_{cb}$ ; the output current and voltage are  $i_o$  and  $V_o$ ; voltage from point a to b is  $V_{ab}$ ; and transformer's turns ratio is  $n$ . Figure 2-1(b) presents the operation principle of conventional control strategy [75], in which driving signals for  $S_1 - S_4$  are  $d_{rv1} - d_{rv4}$  and  $d_1, d_2$  are duty cycles during one switching time period  $T_s$ . Several assumptions are used to simplify following analysis: 1)  $L_o$  is regarded as a constant current source; 2)  $S_1 - S_4$  are considered to be ideal, so impacts from parasitic capacitors can be ignored; 3)  $i_{in}$  is regarded to be constant because of impact from total inductance of input power supply plus input line on  $i_{in}$ .



(a)



(b)

Figure 2-1 (a) Circuit structure. (b) Conventional control strategy [75].

Based on Figure 2-1(b), the expression of  $i_{c1}$  and  $i_{c2}$  can be given as

$$i_{c1} = \begin{cases} -i_{in} & t_0 \leq t < t_2 \\ i_p - i_{in} & t_2 \leq t < t_7 \\ -i_{in} & t_7 \leq t < t_{13} \end{cases} \quad (2.1)$$

$$i_{c2} = \begin{cases} i_p - i_{in} & t_0 \leq t < t_9 \\ -i_{in} & t_9 \leq t < t_{13} \end{cases} \quad (2.2)$$

In addition, the expression of  $i_p$  can be given as

$$i_p = \begin{cases} -\frac{i_o}{n} & t_0 \leq t < t_2 \\ -\frac{i_o}{n} + \frac{V_{in}}{2 \cdot L_r} \cdot (t - t_2) & t_2 \leq t < t_6 \\ \frac{i_o}{n} & t_6 \leq t < t_9 \\ \frac{i_o}{n} - \frac{V_{in}}{2 \cdot L_r} \cdot (t - t_9) & t_9 \leq t < t_{12} \\ -\frac{i_o}{n} & t_{12} \leq t < t_{13} \end{cases} \quad (2.3)$$

Substituting (2.3) into (2.1) and (2.2),  $i_{c1}$  and  $i_{c2}$  can be rewritten as

$$i_{c1} = \begin{cases} -i_{in} & t_0 \leq t < t_2 \\ \frac{V_{in}}{2 \cdot L_r} \cdot (t - t_2) - \frac{i_o}{n} - i_{in} & t_2 \leq t < t_6 \\ \frac{i_o}{n} - i_{in} & t_6 \leq t < t_7 \\ -i_{in} & t_7 \leq t < t_{13} \end{cases} \quad (2.4)$$

$$i_{c2} = \begin{cases} -\frac{i_o}{n} - i_{in} & t_0 \leq t < t_2 \\ \frac{V_{in}}{2 \cdot L_r} \cdot (t - t_2) - \frac{i_o}{n} - i_{in} & t_2 \leq t < t_6 \\ \frac{i_o}{n} - i_{in} & t_6 \leq t < t_9 \\ -i_{in} & t_9 \leq t < t_{13} \end{cases} \quad (2.5)$$

Time periods  $[t_2-t_6]$  and  $[t_9-t_{12}]$  in Figure 2-1(b) are the same and obtained by

$$t_6 - t_2 = t_{12} - t_9 = \frac{4 \cdot L_r \cdot i_o}{n \cdot V_{in}} \quad (2.6)$$

Based on (2.4) ~ (2.6), under conventional control strategy, root-mean-square (RMS) value of  $i_{c1}$ ,  $i_{c2}$  named  $i_{c1\_rms\_con}$ ,  $i_{c2\_rms\_con}$  are obtained by (2.7) and (2.8).

$$i_{c1\_rms\_con} = \sqrt{i_{in}^2 + \frac{i_o^2 \cdot d_1}{n^2} + \frac{8 \cdot L_r \cdot i_{in} \cdot i_o^2}{n^2 \cdot V_{in} \cdot T_s} - \frac{2 \cdot i_{in} \cdot i_o \cdot d_1}{n} - \frac{8 \cdot L_r \cdot i_o^3}{3 \cdot n^3 \cdot V_{in} \cdot T_s}} \quad (2.7)$$

$$i_{c2\_rms\_con} = \sqrt{i_{in}^2 + \frac{i_o^2 \cdot d_2}{n^2} + \frac{8 \cdot L_r \cdot i_{in} \cdot i_o^2}{n^2 \cdot V_{in} \cdot T_s} - \frac{2 \cdot i_{in} \cdot i_o \cdot d_1}{n} - \frac{8 \cdot L_r \cdot i_o^3}{3 \cdot n^3 \cdot V_{in} \cdot T_s}} \quad (2.8)$$

Based on (2.7) and (2.8), the deviation between  $i_{c1\_rms\_con}$ ,  $i_{c2\_rms\_con}$  named  $\Delta i_{c\_rms\_con}$  is (2.9).

$$\Delta i_{c\_rms\_con} = \left| i_{c1\_rms\_con} - i_{c2\_rms\_con} \right| = \frac{i_o^2 \cdot (d_2 - d_1)}{n^2 \cdot (i_{c1\_rms\_con} + i_{c2\_rms\_con})} \quad (2.9)$$

In (2.7) and (2.8),  $i_{c1\_rms\_con}$  and  $i_{c2\_rms\_con}$  are imbalanced.

### 2.1.2. ZVS CONTROL STRATEGY

Figure 2-2 presents proposed ZVS strategy for FS-HBTL isolated DC/DC converter. In Figure 2-2,  $d_{rv1}$ - $d_{rv4}$  are driving signals for  $S_1$ - $S_4$ ;  $d_1$  is duty cycle in one switching time period; and  $d_{loss}$  is duty cycle loss.

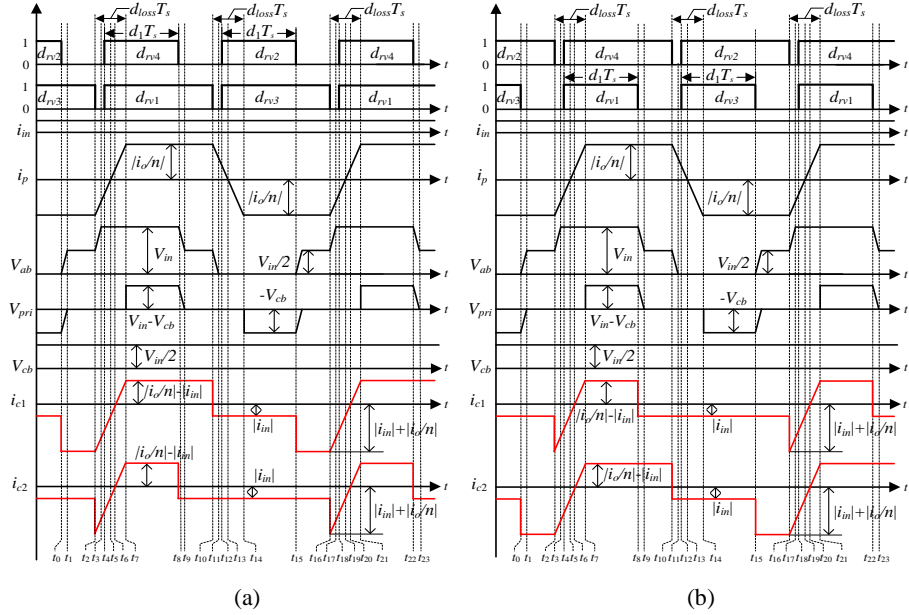


Figure 2-2 Proposed ZVS strategy. (a) Operation mode I. (b) Operation mode II.

Under operation mode I, duty cycle of  $d_{rv1}$ ,  $d_{rv3}$  are 0.5, and duty cycle of  $d_{rv2}$ ,  $d_{rv4}$  are  $d_1$ . Contrarily, under operation mode II, duty cycle of  $d_{rv2}$ ,  $d_{rv4}$  are 0.5, and duty cycle of  $d_{rv1}$ ,  $d_{rv3}$  are  $d_1$ .  $d_1$  should be smaller than 0.5. From Figure 2-2, it can be seen that  $i_{c1}$  and  $i_{c2}$  in two operation modes are just opposite. Furthermore,  $i_{c1}$  is bigger than  $i_{c2}$  under operation mode I, contrarily  $i_{c2}$  is bigger than  $i_{c1}$  under operation mode II. Therefore, major difference between two operation modes is two input capacitors' currents.

### 2.1.3. PSM STRATEGY

Based on major difference of two operation modes, a PSM strategy is proposed to balance  $i_{c1}$  and  $i_{c2}$  through swapping two proposed operation modes in each switch time period (presented in Figure 2-3). Under proposed PSM strategy, operation mode I is utilized during first switching time period, and operation mode II is utilized during second switching time period. Therefore, proposed PSM strategy would balance  $i_{c1}$  and  $i_{c2}$  during every two switching time periods.

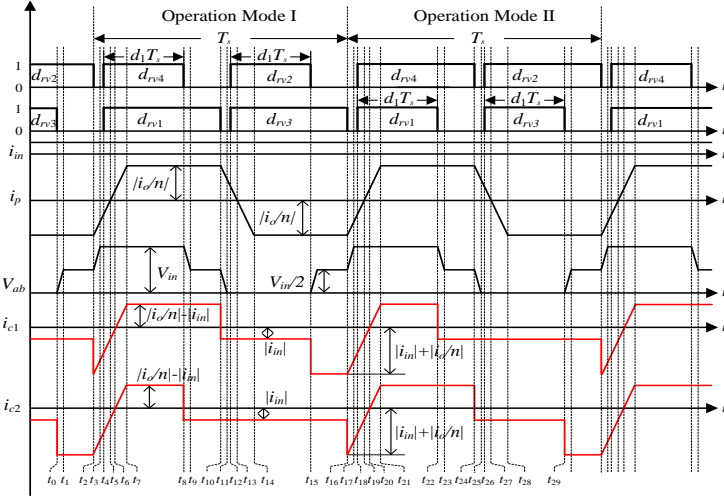


Figure 2-3 Proposed PSM strategy [100].

In Figure 2-3,  $i_{c1}$  and  $i_{c2}$  can be given as (2.10) and (2.11);  $i_p$  can be given as (2.12).

$$i_{c1} = \begin{cases} -i_{in} & t_0 \leq t < t_2 \\ i_p - i_{in} & t_2 \leq t < t_{10} \\ -i_{in} & t_{10} \leq t < t_{15} \\ i_p - i_{in} & t_{15} \leq t < t_{22} \\ -i_{in} & t_{22} \leq t < t_{29} \end{cases} \quad (2.10)$$

$$i_{c2} = \begin{cases} i_p - i_{in} & t_0 \leq t < t_8 \\ -i_{in} & t_8 \leq t < t_{16} \\ i_p - i_{in} & t_{16} \leq t < t_{24} \\ -i_{in} & t_{24} \leq t < t_{29} \end{cases} \quad (2.11)$$

$$i_p = \begin{cases} -\frac{i_o}{n} & t_0 \leq t < t_2 \\ -\frac{i_o}{n} + \frac{V_{in}}{2 \cdot L_r} \cdot (t - t_2) & t_2 \leq t < t_7 \\ \frac{i_o}{n} & t_7 \leq t < t_{10} \\ \frac{i_o}{n} - \frac{V_{in}}{2 \cdot L_r} \cdot (t - t_2) & t_{10} \leq t < t_{14} \\ -\frac{i_o}{n} & t_{14} \leq t < t_{15} \end{cases} \quad (2.12)$$

$i_{c1}$ ,  $i_{c2}$  are rewritten as (2.13) by substituting (2.12) into (2.10) and (2.11).

$$i_{c1} = \begin{cases} -i_{in} & t_0 \leq t < t_2 \\ \frac{V_{in}}{2 \cdot L_r} \cdot (t - t_2) - \frac{i_o}{n} - i_{in} & t_2 \leq t < t_7 \\ \frac{i_o}{n} - i_{in} & t_7 \leq t < t_{10} \\ -i_{in} & t_{10} \leq t < t_{15} \\ -\frac{i_o}{n} - i_{in} & t_{15} \leq t < t_{16} \\ \frac{V_{in}}{2 \cdot L_r} \cdot (t - t_2) - \frac{i_o}{n} - i_{in} & t_{16} \leq t < t_{21} \\ \frac{i_o}{n} - i_{in} & t_{21} \leq t < t_{22} \\ -i_{in} & t_{22} \leq t < t_{29} \end{cases} \quad (2.13)$$

$$i_{c2} = \begin{cases} -\frac{i_o}{n} - i_{in} & t_0 \leq t < t_2 \\ \frac{V_{in}}{2 \cdot L_r} \cdot (t - t_2) - \frac{i_o}{n} - i_{in} & t_2 \leq t < t_7 \\ \frac{i_o}{n} - i_{in} & t_7 \leq t < t_8 \\ -i_{in} & t_8 \leq t < t_{16} \\ \frac{V_{in}}{2 \cdot L_r} \cdot (t - t_2) - \frac{i_o}{n} - i_{in} & t_{16} \leq t < t_{21} \\ \frac{i_o}{n} - i_{in} & t_{21} \leq t < t_{24} \\ -i_{in} & t_{24} \leq t < t_{29} \end{cases} \quad (2.14)$$

Time periods  $[t_2 - t_7]$  and  $[t_{16} - t_{21}]$  in Figure 2-3 are the same as (2.15).

$$t_7 - t_2 = t_{21} - t_{16} = \frac{4 \cdot L_r \cdot i_o}{n \cdot V_{in}} \quad (2.15)$$

Based on (2.13) ~ (2.15), RMS value of  $i_{c1}$ ,  $i_{c2}$  under proposed strategy named  $i_{c1\_rms\_pro}$ ,  $i_{c2\_rms\_pro}$  are

$$i_{c1\_rms\_pro} = i_{c2\_rms\_pro} = \sqrt{i_{in}^2 + \frac{i_o^2}{2 \cdot n^2} + \frac{8 \cdot L_r \cdot i_{in} \cdot i_o^2}{n^2 \cdot V_{in} \cdot T_s} - \frac{2 \cdot i_{in} \cdot i_o \cdot d_1}{n} - \frac{8 \cdot L_r \cdot i_o^3}{3 \cdot n^3 \cdot V_{in} \cdot T_s}} \quad (2.16)$$

From Table 2-1, it could be obtained that: 1) under conventional strategy,  $i_{c1\_rms\_con}$ ,  $i_{c2\_rms\_con}$  are unbalanced, and  $i_{c1\_rms\_con}$  is smaller than  $i_{c2\_rms\_con}$  because  $d_2$  is higher than  $d_1$  in normal operations; 2) in proposed strategy,  $i_{c1\_rms\_pro}$ ,  $i_{c2\_rms\_pro}$  become the same, which means that proposed strategy can eliminate two input capacitors' current imbalance.

By substituting parameters in Table 2-2 into (2.7), (2.8), and (2.16), Figures 2-4 and 2-5 can be obtained. Figure 2-4 presents calculated RMS value of  $i_{c1}$ ,  $i_{c2}$ . Figure 2-5 presents results about deviation  $\Delta i_{c\_rms\_con}$  calculated by (2.9).

Table 2-1 Calculation formulas about RMS value of  $i_{c1}$ ,  $i_{c2}$

Control Strategy	RMS Value	Theoretical Calculation Formula
Conventional Control Strategy	$i_{c1\_rms\_con}$	$\sqrt{i_{in}^2 + \frac{i_o^2 \cdot d_1}{n^2} + \frac{8 \cdot L_r \cdot i_{in} \cdot i_o^2}{n^2 \cdot V_{in} \cdot T_s} - \frac{2 \cdot i_{in} \cdot i_o \cdot d_1}{n} - \frac{8 \cdot L_r \cdot i_o^3}{3 \cdot n^3 \cdot V_{in} \cdot T_s}}$
	$i_{c2\_rms\_con}$	$\sqrt{i_{in}^2 + \frac{i_o^2 \cdot d_2}{n^2} + \frac{8 \cdot L_r \cdot i_{in} \cdot i_o^2}{n^2 \cdot V_{in} \cdot T_s} - \frac{2 \cdot i_{in} \cdot i_o \cdot d_1}{n} - \frac{8 \cdot L_r \cdot i_o^3}{3 \cdot n^3 \cdot V_{in} \cdot T_s}}$
	$\Delta i_{c\_rms\_con}$	$\frac{i_o^2 \cdot (d_2 - d_1)}{n^2 \cdot (i_{c1\_rms\_con} + i_{c2\_rms\_con})}$
Proposed Control Strategy	$i_{c1\_rms\_pro}$ $i_{c2\_rms\_pro}$	$\sqrt{i_{in}^2 + \frac{i_o^2}{2 \cdot n^2} + \frac{8 \cdot L_r \cdot i_{in} \cdot i_o^2}{n^2 \cdot V_{in} \cdot T_s} - \frac{2 \cdot i_{in} \cdot i_o \cdot d_1}{n} - \frac{8 \cdot L_r \cdot i_o^3}{3 \cdot n^3 \cdot V_{in} \cdot T_s}}$

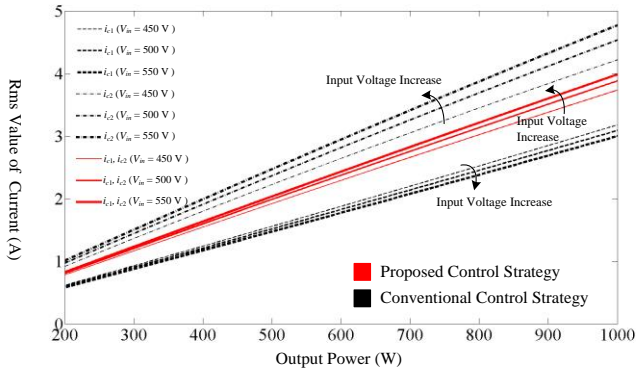


Figure 2-4 Calculated RMS value of  $i_{c1}$ ,  $i_{c2}$  ( $V_o = 50V$ ).



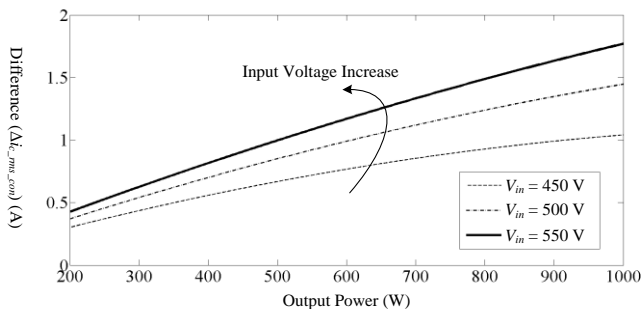


Figure 2-5 Calculated deviations between RMS value of  $i_{c1}$ ,  $i_{c2}$  under the conventional control strategy ( $V_o = 50V$ ).

### 2.1.4. SIMULATION AND EXPERIMENTAL VERIFICATION

#### A. Simulation verification

Table 2-2 presents parameters of simulation model. Figure 2-6 presents simulation results. As marked in Figure 2-6(b),  $i_{c1}$ ,  $i_{c2}$  are same during every two switching time periods under proposed strategy. In Fig. 2-6,  $i_{c1\_rms\_con}$ ,  $i_{c2\_rms\_con}$  are 3.05 A and 5.11 A respectively, but  $i_{c1\_rms\_pro}$ ,  $i_{c2\_rms\_pro}$  are both 4.2 A.

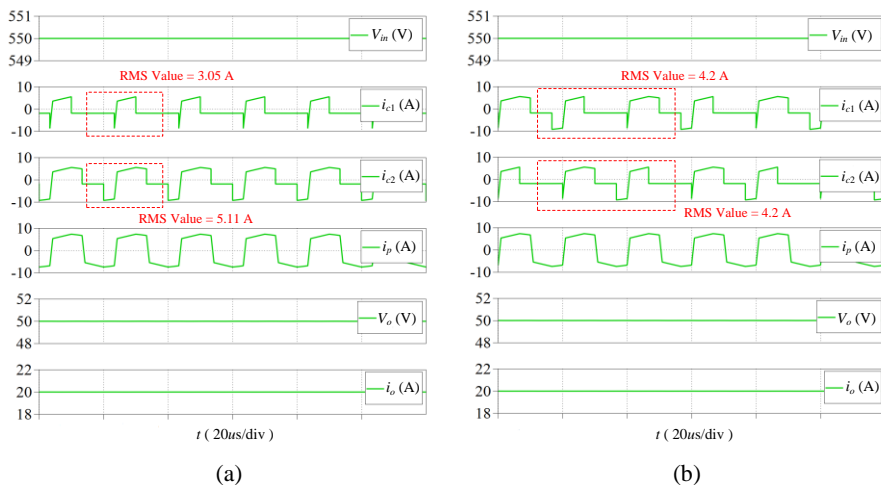


Figure 2-6 Simulation results ( $V_{in} = 550 V$ ,  $V_o = 50 V$ ,  $P_o = 1 kW$ ). (a) Conventional strategy. (b) Proposed strategy.

### B. Experimental verification

Table 2-2 presents parameters of established prototype; Figure 2-7 presents the hardware of established prototype (1 kW).

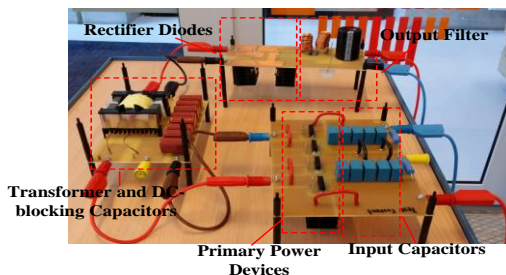


Figure 2-7 Hardware of established prototype.

Table 2-2 Parameters of simulation model and experimental prototype

Description	Parameter
Power Switches $S_1 - S_4$	SPW47N60C3
Rectifier Diodes $D_{r1} - D_{r4}$	MBR40250TG
Turns Ratio of Transformer $T_r$	25 : 8
Leakage Inductance $L_r$ ( $\mu$ H)	20.7
Output Filter Capacitor $C_o$ ( $\mu$ F)	470
Output Filter Inductor $L_o$ ( $\mu$ H)	140
Input Capacitors $C_1$ and $C_2$ ( $\mu$ F)	14.4
DC-blocking Capacitor $C_b$ ( $\mu$ F)	12
Switching Frequency (kHz)	50
Dead Time (ns)	400
Input Inductance ( $\mu$ H) (Including the output inductance of the input power supply and inductance of the input line)	60

Figure 2-8 illustrates control block of proposed strategy.

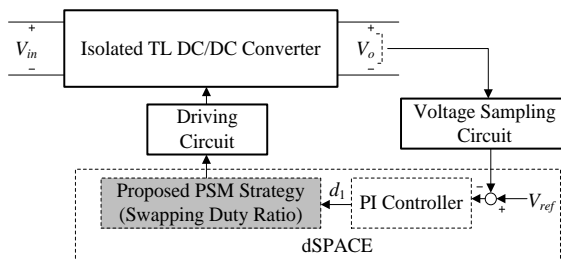
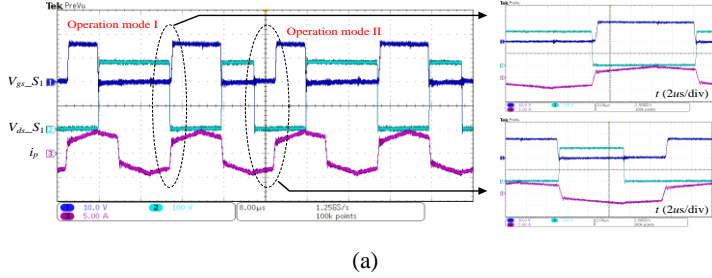
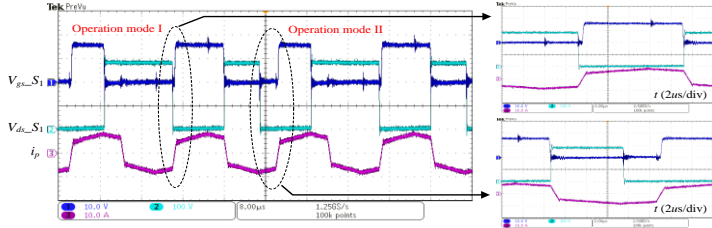


Figure 2-8 Control block of proposed PSM strategy.

Figures 2-9 and 2-10 show ZVS achievement performances in proposed control strategy, in which  $V_{ds\_S1}$ ,  $V_{ds\_S3}$  are drain-source voltage of  $S_1$ ,  $S_3$  and  $V_{gs\_S1}$ ,  $V_{gs\_S3}$  are driving signal of  $S_1$ ,  $S_3$ .

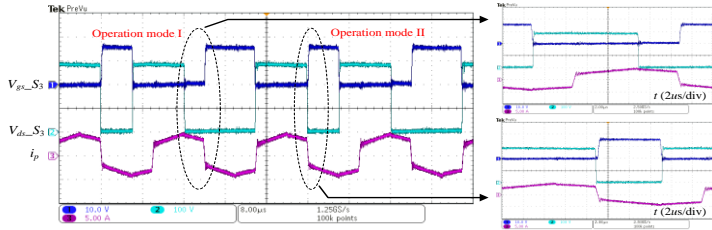


(a)

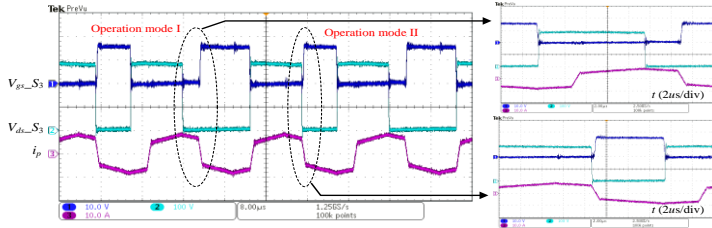


(b)

Figure 2-9 ZVS performance of  $S_1$  ( $V_{in} = 550$  V,  $V_o = 50$  V). (a)  $P_o = 500$  W. (b)  $P_o = 1$  kW.



(a)



(b)

Figure 2-10 ZVS performance of  $S_3$  ( $V_{in} = 550$  V,  $V_o = 50$  V). (a)  $P_o = 500$  W. (b)  $P_o = 1$  kW.

Figures 2-11 ~ 2-13 present experimental results. In Figure 2-13 ( $P_o = 1$  kW),  $i_{c1\_rms\_con}$ ,  $i_{c2\_rms\_con}$  are 3.16 A and 5.18 A respectively;  $\Delta i_{c\_rms\_con}$  2.02 A; but  $i_{c1\_rms\_pro}$ ,  $i_{c2\_rms\_pro}$  are both 4.37 A, which validates that proposed PSM strategy can eliminate current imbalance among input capacitors caused by conventional strategy.

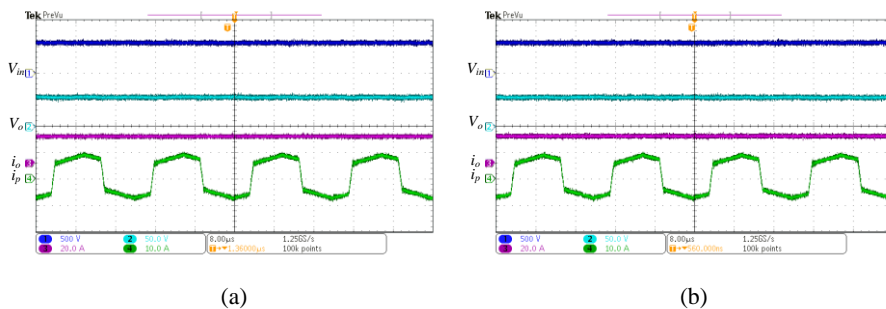


Figure 2-11 Experimental results of  $V_{in}$ ,  $V_o$ ,  $i_o$ , and  $i_p$  ( $V_{in} = 550$  V,  $V_o = 50$  V,  $P_o = 1$  kW) [100]. (a) Conventional strategy. (b) Proposed strategy.

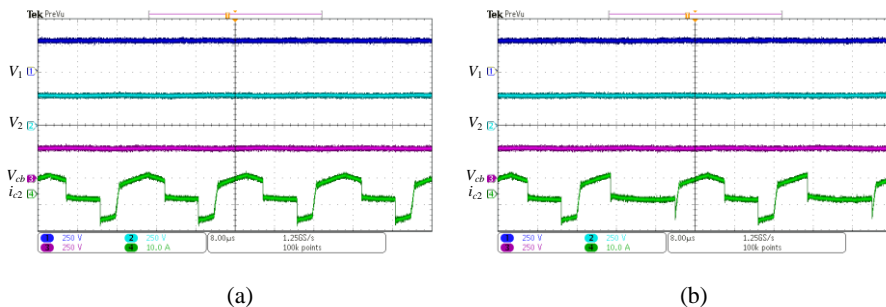


Figure 2-12 Experimental results of  $V_1$ ,  $V_2$ ,  $V_{cb}$ , and  $i_{c2}$  ( $V_{in} = 550$  V,  $V_o = 50$  V,  $P_o = 1$  kW) [100]. (a) Conventional strategy. (b) Proposed strategy.

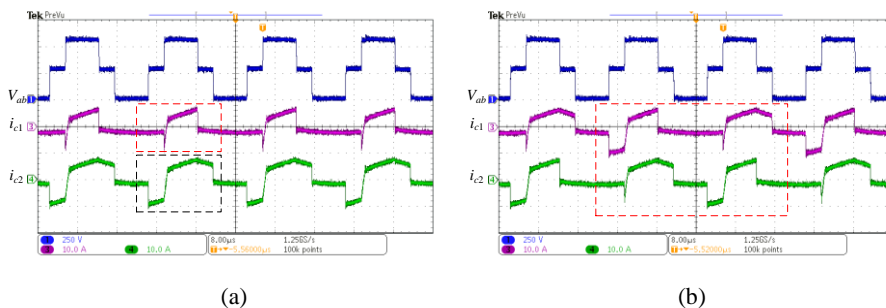


Figure 2-13 Experimental results of  $V_{ab}$ ,  $i_{c1}$ , and  $i_{c2}$  ( $V_{in} = 550$  V,  $V_o = 50$  V,  $P_o = 1$  kW) [100]. (a) Conventional strategy. (b) Proposed strategy.

Figure 2-14 demonstrates experimental RMS value about  $i_{c1}$ ,  $i_{c2}$ .

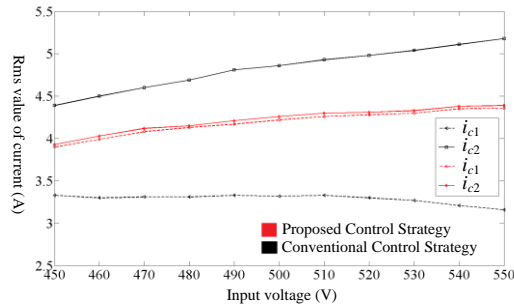


Figure 2-14 Experimental RMS value of  $i_{c1}$ ,  $i_{c2}$  ( $V_o = 50$  V,  $P_o = 1$  kW).

Figure 2-15 presents the dynamic performance.

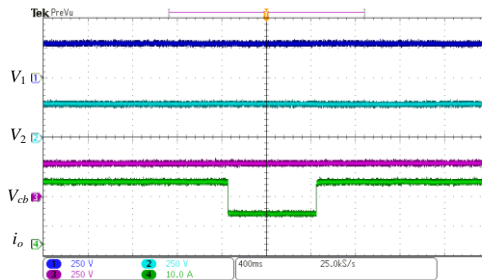


Figure 2-15 Dynamic performances under load changes (1 kW to 500 W to 1 kW) ( $V_{in} = 550$  V  $V_o = 50$  V).

Figure 2-16 presents experimental efficiency results. It is noted that the efficiency results are calculated by (measured  $V_o \times$  measured  $i_o$ ) / (measured  $V_{in} \times$  measured  $i_{in}$ ).

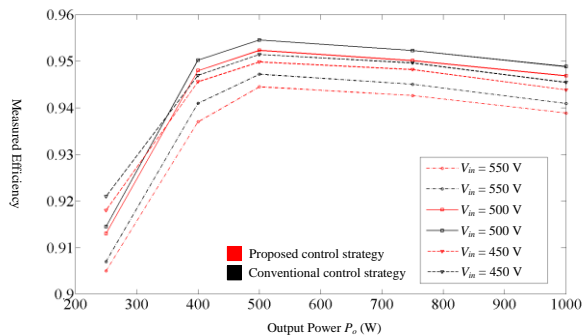


Figure 2-16 Experimental efficiency results ( $V_o = 50$  V).

## 2.2. IPOP TL ISOLATED DC/DC CONVERTERS

### 2.2.1. CIRCUIT STRUCTURE

Figure 2-17 presents the IPOP TL IDCs including dual FS-HBTL IDCs (named Module I and Module II). In Figure 2-17,  $V_{in}$  is input voltage;  $C_1$  and  $C_2$  are input capacitors to split  $V_{in}$  into two voltages  $V_1$  and  $V_2$ ; and  $C_o$  is filter capacitor. In Module I,  $S_1$ - $S_4$  are power switches;  $D_1$ - $D_4$  are power diodes;  $T_{r1}$  is isolated transformer;  $L_{r1}$  is leakage inductance of  $T_{r1}$ ;  $C_{b1}$  is DC-blocking capacitor;  $D_{r1}$ - $D_{r4}$  are four rectifier diodes;  $L_{o1}$  is filter inductor. Module II is the same as Module I. In Figure 2-17,  $i_{in}$  is input current; current through  $C_1$  and  $C_2$  are  $i_{c1}$  and  $i_{c2}$  respectively; primary current of  $T_{r1}$  and  $T_{r2}$  are  $i_{p1}$  and  $i_{p2}$ ; current on  $L_{o1}$  and  $L_{o2}$  are  $i_{Lo1}$  and  $i_{Lo2}$ ; voltage on  $C_{b1}$  and  $C_{b2}$  are  $V_{cb1}$  and  $V_{cb2}$ ; output voltage and current are  $V_o$  and  $i_o$ ; voltage from point  $a$  to  $b$  is  $V_{ab}$ ; the voltage from point  $c$  to  $d$  is  $V_{cd}$ ; turns ratios in  $T_{r1}$  and  $T_{r2}$  are  $n_1$  and  $n_2$ .

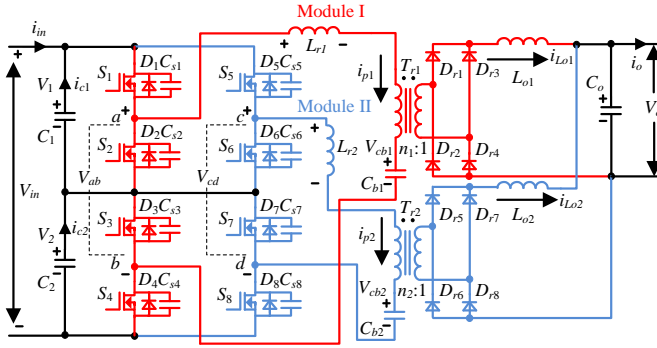


Figure 2-17 Circuit structure.

### 2.2.2. WORKING PRINCIPLE

Some assumptions are used to simplify following analysis: 1)  $L_{o1}$  and  $L_{o2}$  are the same and regarded as constant current sources; 2)  $S_1 - S_8$  and  $D_1 - D_8$  are ideal; 3)  $C_1$ ,  $C_2$ ,  $C_{b1}$ , and  $C_{b2}$  are regarded as constant voltage sources and  $C_1 = C_2 = C_{in}$ ,  $C_{b1} = C_{b2} = C_b$ ,  $V_1 = V_2 = V_{in}/2$ ,  $V_{cb1} = V_{cb2} = V_{cb} = V_{in}/2$ ; 4) the parameters of  $T_{r1}$  and  $T_{r2}$  are identical:  $n_1 = n_2 = n$  and  $L_{r1} = L_{r2} = L_r$ ; 5)  $i_{in}$  is regarded to be constant because of impact from inductance (input power supply's output inductance plus input line inductance) on  $i_{in}$ .

Figure 2-18 presents working principle of proposed converters. In Figure 18,  $d_{rv1}$ - $d_{rv8}$  are driving signals for  $S_1$ - $S_8$ ,  $d_1$ - $d_2$  are duty cycles during one switching time period. As drawn by color in Figure 2-18(a),  $i_{c1}$  and  $i_{c2}$  are unbalanced without interleaving control strategy. On contrary, under interleaving control strategy,  $i_{c1}$  and  $i_{c2}$  become much smaller and balanced.

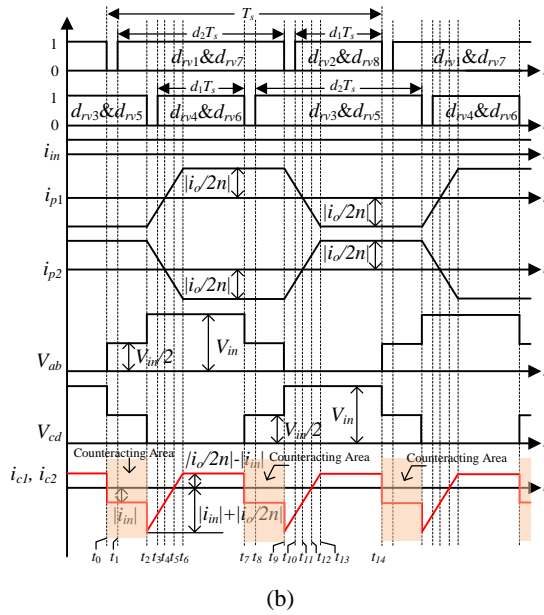
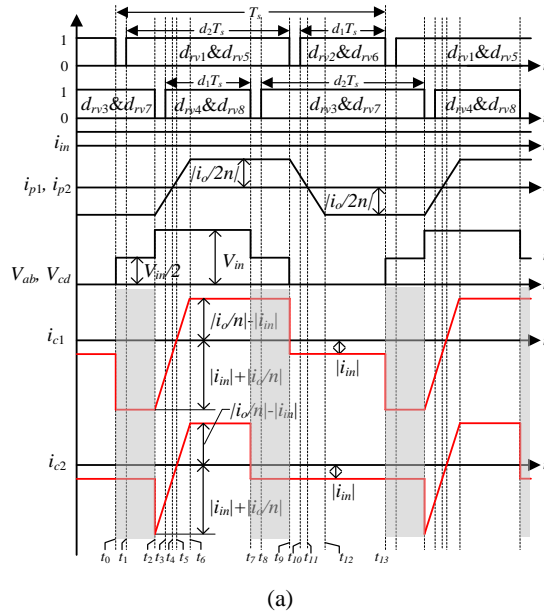


Figure 2-18 (a) Without interleaving control strategy. (b) With interleaving control strategy. [101]

Equivalent circuits are presented in Figure 2-19 to explain proposed converters' working process.

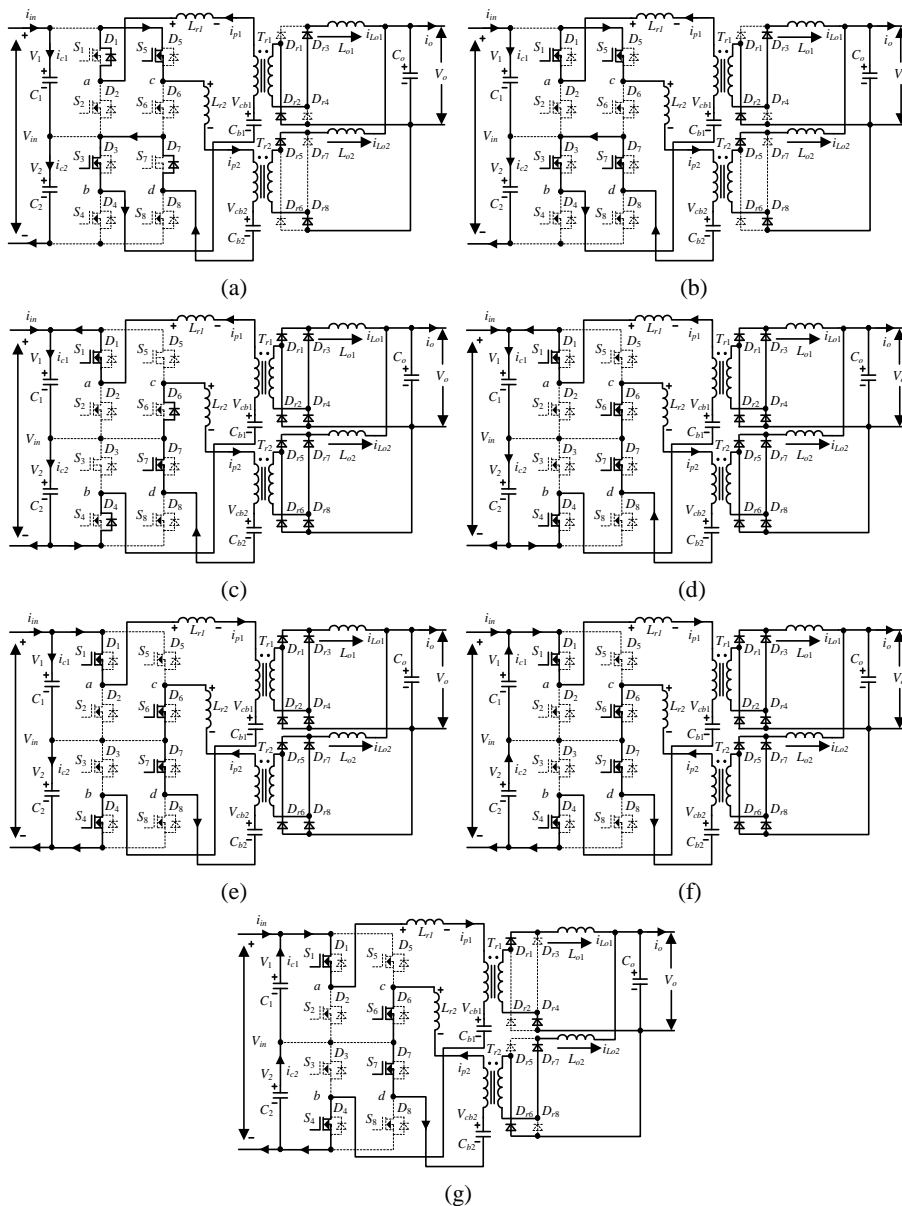


Figure 2-19 Equivalent circuits with interleaving control strategy [101]. (a)  $[t_0-t_1]$ . (b)  $[t_1-t_2]$ . (c)  $[t_2-t_3]$ . (d)  $[t_3-t_4]$ . (e)  $[t_4-t_5]$ . (f)  $[t_5-t_6]$ . (g)  $[t_6-t_7]$ .



### 2.2.3. CURRENTS ON INPUT CAPACITORS

Based on Figure 2-18(b),  $i_{c1}$  and  $i_{c2}$  can be expressed as

$$i_{c1} = i_{c2} = \begin{cases} -i_{in} & t_0 \leq t < t_2 \\ i_{p1} - i_{in} & t_2 \leq t < t_7 \end{cases} \quad (2.17)$$

$i_{p1}$  and  $i_{p2}$  are given as

$$i_{p1} = -i_{p2} = \begin{cases} -\frac{i_o}{2 \cdot n} & t_0 \leq t < t_2 \\ -\frac{i_o}{2 \cdot n} + \frac{V_{in}}{2 \cdot L_r} \cdot (t - t_2) & t_2 \leq t < t_6 \\ \frac{i_o}{2 \cdot n} & t_6 \leq t < t_7 \end{cases} \quad (2.18)$$

Substituting (2.18) into (2.17),  $i_{c1}$  and  $i_{c2}$  are rewritten by

$$i_{c1} = i_{c2} = \begin{cases} -i_{in} & t_0 \leq t < t_2 \\ \frac{V_{in}}{2 \cdot L_r} \cdot (t - t_2) - \frac{i_o}{2 \cdot n} - i_{in} & t_2 \leq t < t_6 \\ \frac{i_o}{2 \cdot n} - i_{in} & t_6 \leq t < t_7 \end{cases} \quad (2.19)$$

Time periods  $[t_2-t_6]$  and  $[t_9-t_{13}]$  in Figure 2-18(b) are the same and can be obtained by

$$t_6 - t_2 = t_{13} - t_9 = \frac{2 \cdot L_r \cdot i_o}{n \cdot V_{in}} \quad (2.20)$$

According to (2.19) and (2.20), RMS value of  $i_{c1}$ ,  $i_{c2}$  under interleaving control strategy named  $i_{c1\_rms\_II}$ ,  $i_{c2\_rms\_II}$  are

$$i_{c1\_rms\_II} = i_{c2\_rms\_II} = \sqrt{i_{in}^2 + \frac{i_o^2 \cdot d_1}{2 \cdot n^2} + \frac{4 \cdot L_r \cdot i_{in} \cdot i_o^2}{n^2 \cdot V_{in} \cdot T_s} - \frac{2 \cdot i_{in} \cdot i_o \cdot d_1}{n} - \frac{2 \cdot L_r \cdot i_o^3}{3 \cdot n^3 \cdot V_{in} \cdot T_s}} \quad (2.21)$$

RMS value of  $i_{c1}$ ,  $i_{c2}$  without interleaving control strategy presented in Figure 2-18(a) named  $i_{c1\_rms\_I}$ ,  $i_{c2\_rms\_I}$  are

$$i_{c1\_rms\_I} = \sqrt{i_{in}^2 + \frac{i_o^2 \cdot d_2}{n^2} + \frac{4 \cdot L_r \cdot i_{in} \cdot i_o^2}{n^2 \cdot V_{in} \cdot T_s} - \frac{2 \cdot i_{in} \cdot i_o \cdot d_1}{n} - \frac{4 \cdot L_r \cdot i_o^3}{3 \cdot n^3 \cdot V_{in} \cdot T_s}} \quad (2.22)$$

$$i_{c2\_rms\_I} = \sqrt{i_{in}^2 + \frac{i_o^2 \cdot d_1}{n^2} + \frac{4 \cdot L_r \cdot i_{in} \cdot i_o^2}{n^2 \cdot V_{in} \cdot T_s} - \frac{2 \cdot i_{in} \cdot i_o \cdot d_1}{n} - \frac{4 \cdot L_r \cdot i_o^3}{3 \cdot n^3 \cdot V_{in} \cdot T_s}} \quad (2.23)$$

Based on (2.22) and (2.23), deviation between  $i_{c1\_rms\_I}$ ,  $i_{c2\_rms\_I}$  named  $\Delta i_{c\_rms\_I}$  is

$$\Delta i_{c\_rms\_I} = i_{c1\_rms\_I} - i_{c2\_rms\_I} = \frac{i_o^2 \cdot (d_2 - d_1)}{n^2 \cdot (i_{c1\_rms\_I} + i_{c2\_rms\_I})} \quad (2.24)$$

Table 2-3 Calculation formulas about RMS value of  $i_{c1}$ ,  $i_{c2}$

Control Strategy	RMS Value	Theoretical Calculation Formula
Without the interleaving control strategy	$i_{c1\_rms\_I}$	$\sqrt{i_{in}^2 + \frac{i_o^2 \cdot d_2}{n^2} + \frac{4 \cdot L_r \cdot i_{in} \cdot i_o^2}{n^2 \cdot V_{in} \cdot T_s} - \frac{2 \cdot i_{in} \cdot i_o \cdot d_1}{n} - \frac{4 \cdot L_r \cdot i_o^3}{3 \cdot n^3 \cdot V_{in} \cdot T_s}}$
	$i_{c2\_rms\_I}$	$\sqrt{i_{in}^2 + \frac{i_o^2 \cdot d_1}{n^2} + \frac{4 \cdot L_r \cdot i_{in} \cdot i_o^2}{n^2 \cdot V_{in} \cdot T_s} - \frac{2 \cdot i_{in} \cdot i_o \cdot d_1}{n} - \frac{4 \cdot L_r \cdot i_o^3}{3 \cdot n^3 \cdot V_{in} \cdot T_s}}$
	$\Delta i_{c\_rms\_I}$	$\frac{i_o^2 \cdot (d_2 - d_1)}{n^2 \cdot (i_{c1\_rms\_I} + i_{c2\_rms\_I})}$
With the interleaving control strategy	$i_{c1\_rms\_II}$ , $i_{c2\_rms\_II}$	$\sqrt{i_{in}^2 + \frac{i_o^2 \cdot d_1}{2 \cdot n^2} + \frac{4 \cdot L_r \cdot i_{in} \cdot i_o^2}{n^2 \cdot V_{in} \cdot T_s} - \frac{2 \cdot i_{in} \cdot i_o \cdot d_1}{n} - \frac{2 \cdot L_r \cdot i_o^3}{3 \cdot n^3 \cdot V_{in} \cdot T_s}}$

Through substituting parameters in Table 2-4 to calculation formulas in Table 2-3, calculation results of  $i_{c1\_rms\_I}$ ,  $i_{c2\_rms\_I}$ ,  $i_{c1\_rms\_II}$ , and  $i_{c2\_rms\_II}$  are obtained in Figure 2-20. Fig. 2-20 demonstrates that: 1)  $i_{c1\_rms\_I}$ ,  $i_{c2\_rms\_I}$  are different, but  $i_{c1\_rms\_II}$ ,  $i_{c2\_rms\_II}$  are same; and 2)  $i_{c1\_rms\_II}$ ,  $i_{c2\_rms\_II}$  are much smaller than  $i_{c1\_rms\_I}$ ,  $i_{c2\_rms\_I}$ .

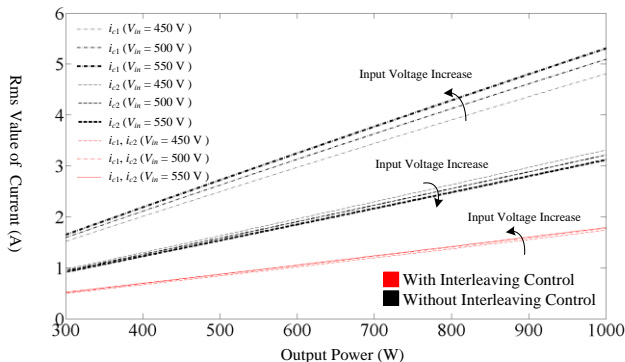


Figure 2-20 Calculation results about RMS value of  $i_{c1}$ ,  $i_{c2}$  ( $V_o = 50\text{ V}$ ).

## 2.2.4. SIMULATION AND EXPERIMENTAL VERIFICATION

### A. Simulation verification

Table 2-4 presents parameters of simulation model. Figure 2-21 presents simulation results, in which 1)  $i_{c1\_rms\_I}$ ,  $i_{c2\_rms\_I}$  are 5.8 A and 3.2 A respectively; and 2)  $i_{c1\_rms\_II}$ ,  $i_{c2\_rms\_II}$  become the same and decrease to both 1.76 A. Therefore, simulation results verify that  $i_{c1}$ ,  $i_{c2}$  can be effectively balanced and greatly decreased.

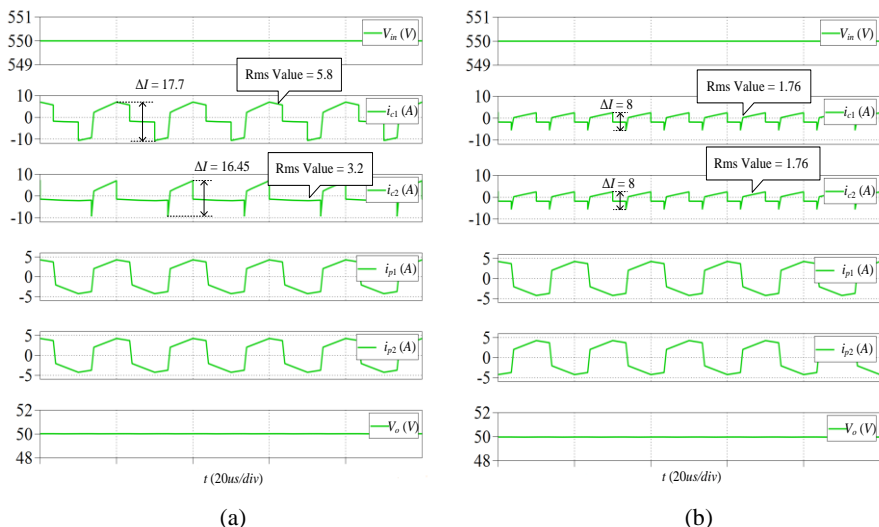


Figure 2-21 Simulation results ( $V_{in} = 550\text{ V}$ ,  $V_o = 50\text{ V}$ , and  $P_o = 1\text{ kW}$ ). (a) Without interleaving control strategy. (b) With interleaving control strategy. [101]

## B. Experimental verification

Table 2-4 presents parameters of established prototype. Figure 2-22 presents built prototype's hardware.

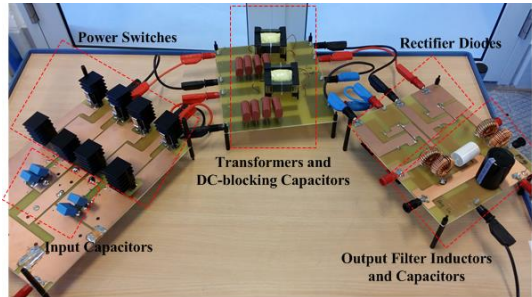


Figure 2-22 Hardware of established prototype.

Table 2-4 Parameters in simulation and experiments

Description	Parameter
Power switches $S_1 - S_8$	SPW47N60C3
Rectifier diodes $D_{r1} - D_{r8}$	MBR20200CTG
Turns Ratios of $T_{r1}$ and $T_{r2}$	38 : 13
Leakage Inductances $L_{r1}$ and $L_{r2}$ (uH)	30
Output Filter Capacitor $C_o$ (uF)	470
Output Filter Inductors $L_{o1}$ and $L_{o2}$ (uH)	100
Input Capacitors $C_1$ and $C_2$ (uF)	14.4
DC-blocking Capacitors $C_{b1}$ and $C_{b2}$ (uF)	6
Switching Frequency (kHz)	50
Dead Time (ns)	400

Figures 2-23 ~ 2-26 show experimental results.

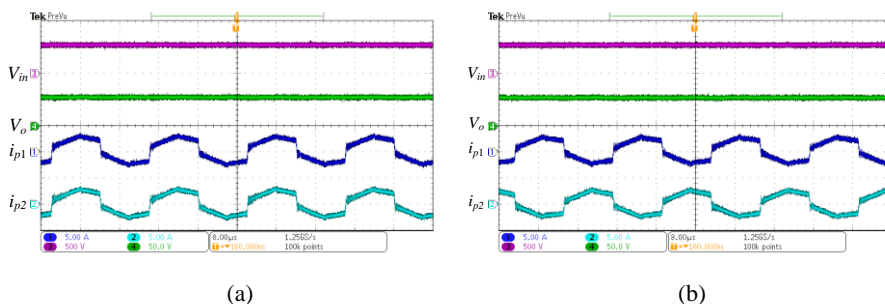


Figure 2-23 Experimental results of  $V_{in}$ ,  $V_o$ ,  $i_{p1}$ , and  $i_{p2}$  under 500 W ( $V_{in} = 550$  V,  $V_o = 50$  V) [101]. (a) Without interleaving control strategy. (b) With interleaving control strategy.

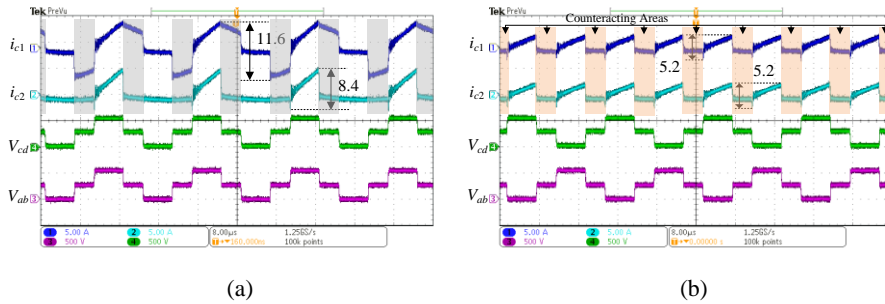


Figure 2-24 Experimental results of  $i_{c1}$ ,  $i_{c2}$ ,  $V_{ab}$ , and  $V_{cd}$  under 500 W ( $V_{in} = 550$  V,  $V_o = 50$  V) [101]. (a) Without interleaving control strategy. (b) With interleaving control strategy.

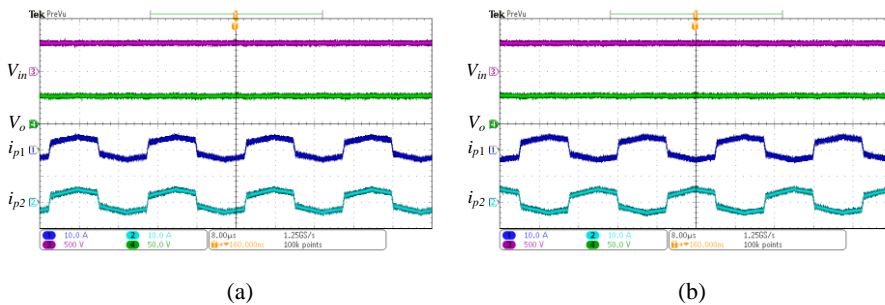


Figure 2-25 Experimental results of  $V_{in}$ ,  $V_o$ ,  $i_{p1}$ , and  $i_{p2}$  under 1 kW ( $V_{in} = 550$  V,  $V_o = 50$  V) [101]. (a) Without interleaving control strategy. (b) With interleaving control strategy.

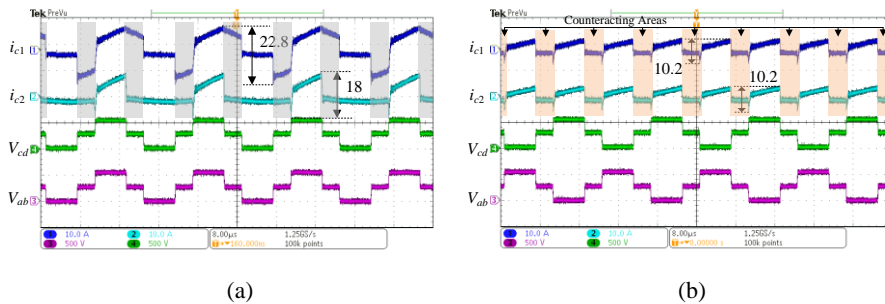


Figure 2-26 Experimental results of  $i_{c1}$ ,  $i_{c2}$ ,  $V_{ab}$ , and  $V_{cd}$  under 1 kW ( $V_{in} = 550$  V,  $V_o = 50$  V) [101]. (a) Without interleaving control strategy. (b) With interleaving control strategy.

When  $P_o$  is 500 W in Figure 2-24,  $i_{c1\_rms\_I}$ ,  $i_{c2\_rms\_I}$  are 3.2 A and 1.68 A respectively; contrarily  $i_{c1\_rms\_II}$ ,  $i_{c2\_rms\_II}$  are almost the same and decrease to 0.978 A and 0.971 A respectively. When  $P_o$  is 1 kW in Figure 2-26,  $i_{c1\_rms\_I}$ ,  $i_{c2\_rms\_I}$  are 5.6 A and 3.19 A, so deviation between them is 2.41 A; contrarily  $i_{c1\_rms\_II}$ ,  $i_{c2\_rms\_II}$  are almost same and reduce to 1.69 A and 1.68 A respectively.

Figure 2-27 presents experimental results and theoretical calculations of RMS value of  $i_{c1}$  and  $i_{c2}$ , in which the differences between the theoretical calculation and experimental results are very slight.

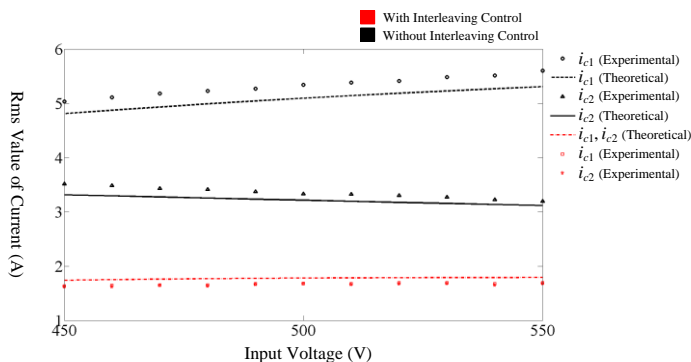


Figure 2-27 RMS value of  $i_{c1}$  and  $i_{c2}$  ( $V_o = 50$  V and  $P_o = 1$  kW).

## 2.3. SUMMARY

Firstly, this chapter proposes a ZVS strategy including a PSM strategy for FS-HBTL isolated DC/DC converter to eliminate current imbalance among input capacitors, which can thus balance the two input capacitors' thermal stress and lifetime. Simulation and experimental results both validate proposed ZVS strategy and modulation strategy. The papers related to these contents are J2 and C3.

Secondly, this chapter proposes IPOP TL IDCs to balance and minimize two input capacitors' currents, which can thus 1) reduce input capacitors' size; and 2) balance two input capacitors' thermal stress and lifetime. Simulation and experimental results both validate proposed converters.

The papers related to this chapter are J1 and C2.

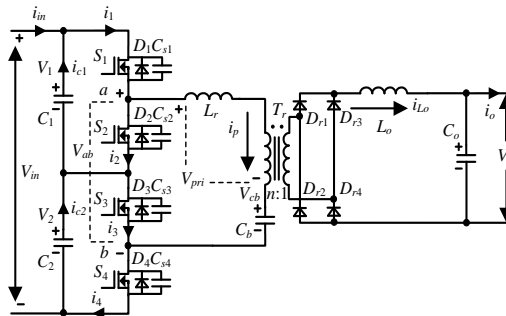
# CHAPTER 3. IMPROVING POWER DEVICE PERFORMANCE

This chapter aims at improving power device performance of TL-IDCs. The proposed PSM strategy can be also utilized for TL-IDCs with asymmetrical modulation strategy to balance power devices' currents. This chapter analyzes FS-HBTL isolated DC/DC converter [75] as an instance to illustrate current imbalance issue and power devices' currents under proposed PSM strategy. The analysis about current imbalance issue and working process under proposed PSM strategy of other TL-IDCs [94-96] (mentioned in Section 1.3.2) are similar.

## 3.1. POWER DEVICE CURRENT IMBALANCE ISSUE

Figure 3-1(a) presents the FS-HBTL isolated DC/DC converter's circuit structure [75] and Figure 3-1(b) presents asymmetrical modulation strategy [75]. In Figure 3-1(a),  $V_{in}$  is input voltage;  $C_1$  and  $C_2$  are two input capacitors to split  $V_{in}$  into two voltages  $V_1$  and  $V_2$ ;  $S_1 - S_4$  and  $D_1 - D_4$  are power switches and diodes;  $T_r$  is isolated transformer;  $L_r$  is the leakage inductance of  $T_r$ ;  $C_{s1} - C_{s4}$  are parasitic capacitors of  $S_1 - S_4$ ;  $C_b$  is the DC-blocking capacitor;  $D_{r1} - D_{r4}$  are four output rectifier diodes;  $L_o$  is filter inductor;  $C_o$  is filter capacitor. In Figure 3-1(a), input current is  $i_{in}$ ; primary current on  $T_r$  is  $i_p$ ; currents on  $(S_1, D_1)$ ,  $(S_2, D_2)$ ,  $(S_3, D_3)$ , and  $(S_4, D_4)$  are  $i_1, i_2, i_3$ , and  $i_4$ ; the currents on  $C_1$  and  $C_2$  are  $i_{c1}$  and  $i_{c2}$ ; the current on  $L_o$  is  $i_{Lo}$ ; the voltage on  $C_b$  is  $V_{cb}$ ;  $V_o$  is output voltage;  $i_o$  is output current; voltage from point  $a$  to  $b$  is  $V_{ab}$ ; and the turns ratio of  $T_r$  is  $n$ . In Figure 3-1(b),  $d_{rv1} - d_{rv4}$  are driving signals for  $S_1 - S_4$ ;  $d_1$  and  $d_2$  are duty cycles during one switching time period;  $d_2$  is  $1 - d_1$  when ignoring dead-time.

Some assumptions are used to simplify following analysis: 1)  $L_o$  is regarded as a current source; 2)  $S_1 - S_4$  and  $D_1 - D_4$  are ideal; 3)  $C_1, C_2$ , and  $C_b$  are regarded as constant voltage sources ( $V_{in}/2$ ).



(a)

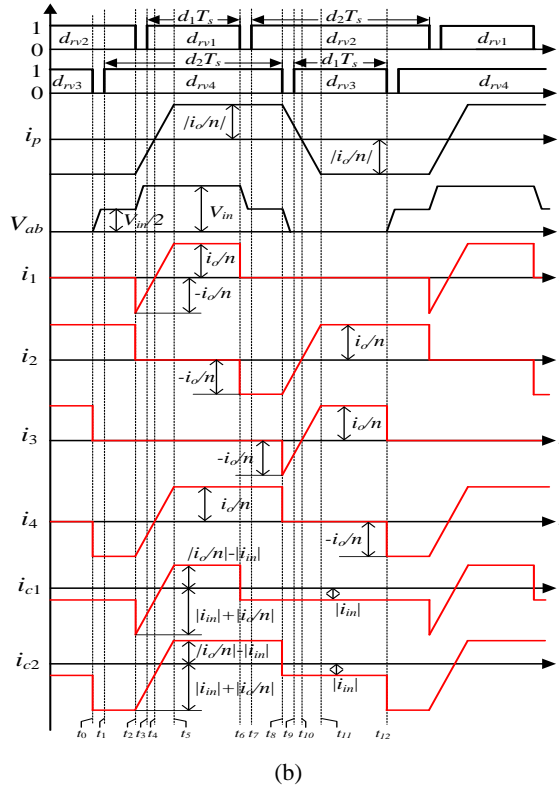


Figure 3-1 (a) Circuit Structure. (b) Asymmetrical modulation strategy [75].

In Figure 3-1(b), current pairs  $(i_1, i_3)$  and  $(i_2, i_4)$  are same during each switching time period. Therefore, only  $i_1, i_2$  are given as

$$i_1 = \begin{cases} -\frac{i_o}{n} + \frac{V_m}{2 \cdot L_r} \cdot t & [t_2 - t_5] \\ \frac{i_o}{n} & [t_5 - t_6] \end{cases} \quad (3.1)$$

$$i_2 = \begin{cases} \frac{i_o}{n} & [t_0 - t_2] \\ -\frac{i_o}{n} & [t_6 - t_8] \\ -\frac{i_o}{n} + \frac{V_m}{2 \cdot L_r} \cdot t & [t_8 - t_{11}] \\ \frac{i_o}{n} & [t_{11} - t_{12}] \end{cases} \quad (3.2)$$

Time periods  $[t_2 - t_5]$  and  $[t_8 - t_{11}]$  are the same and can be calculated by



$$t_5 - t_2 = t_{11} - t_8 = \frac{4 \cdot L_r \cdot i_o}{n \cdot V_{in}} \quad (3.3)$$

Based on (3.1) ~ (3.3), RMS value of  $i_1$ ,  $i_2$ ,  $i_3$ , and  $i_4$  in asymmetrical modulation strategy named  $i_{1\_rms\_c}$ ,  $i_{2\_rms\_c}$ ,  $i_{3\_rms\_c}$ , and  $i_{4\_rms\_c}$  are

$$i_{1\_rms\_c} = i_{3\_rms\_c} = \sqrt{\frac{i_o^2}{n^2} \cdot d_1 - \frac{8 \cdot L_r \cdot i_o^3}{3 \cdot n^3 \cdot V_{in} \cdot T_s}} \quad (3.4)$$

$$i_{2\_rms\_c} = i_{4\_rms\_c} = \sqrt{\frac{i_o^2}{n^2} \cdot d_2 - \frac{8 \cdot L_r \cdot i_o^3}{3 \cdot n^3 \cdot V_{in} \cdot T_s}} \quad (3.5)$$

From (3.4) and (3.5), it can be observed that the current pairs ( $i_{1\_rms\_c}$ ,  $i_{3\_rms\_c}$ ) and ( $i_{2\_rms\_c}$ ,  $i_{4\_rms\_c}$ ) are imbalanced, which thus would cause the power devices' power loss and thermal stress imbalance and undermine converter's reliability.

### 3.2. POWER DEVICES' CURRENTS UNDER PSM STRATEGY

Figure 3-2 shows power devices' currents under proposed PSM strategy, in which  $d_{rv1}$ - $d_{rv4}$  are driving signals for  $S_1$ - $S_4$ ;  $d_1$  is duty cycle during one switching time period;  $d_{loss}$  is duty cycle loss.

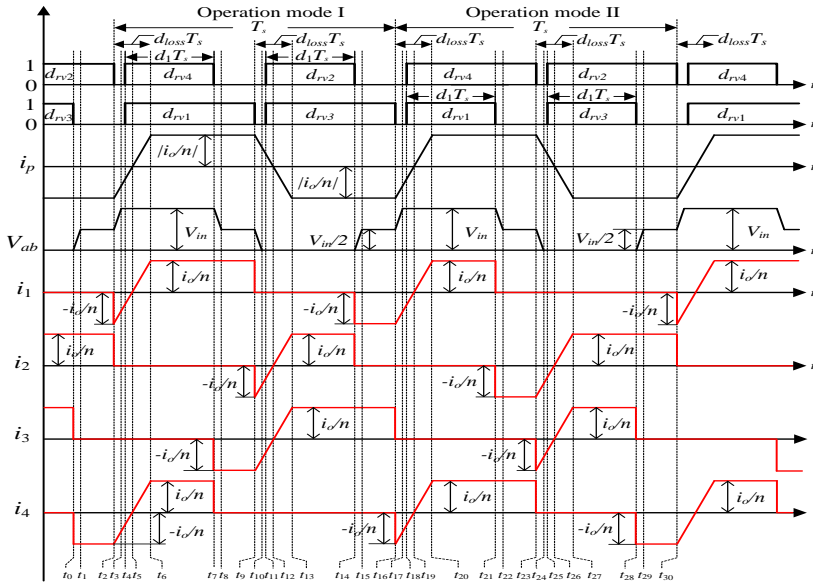
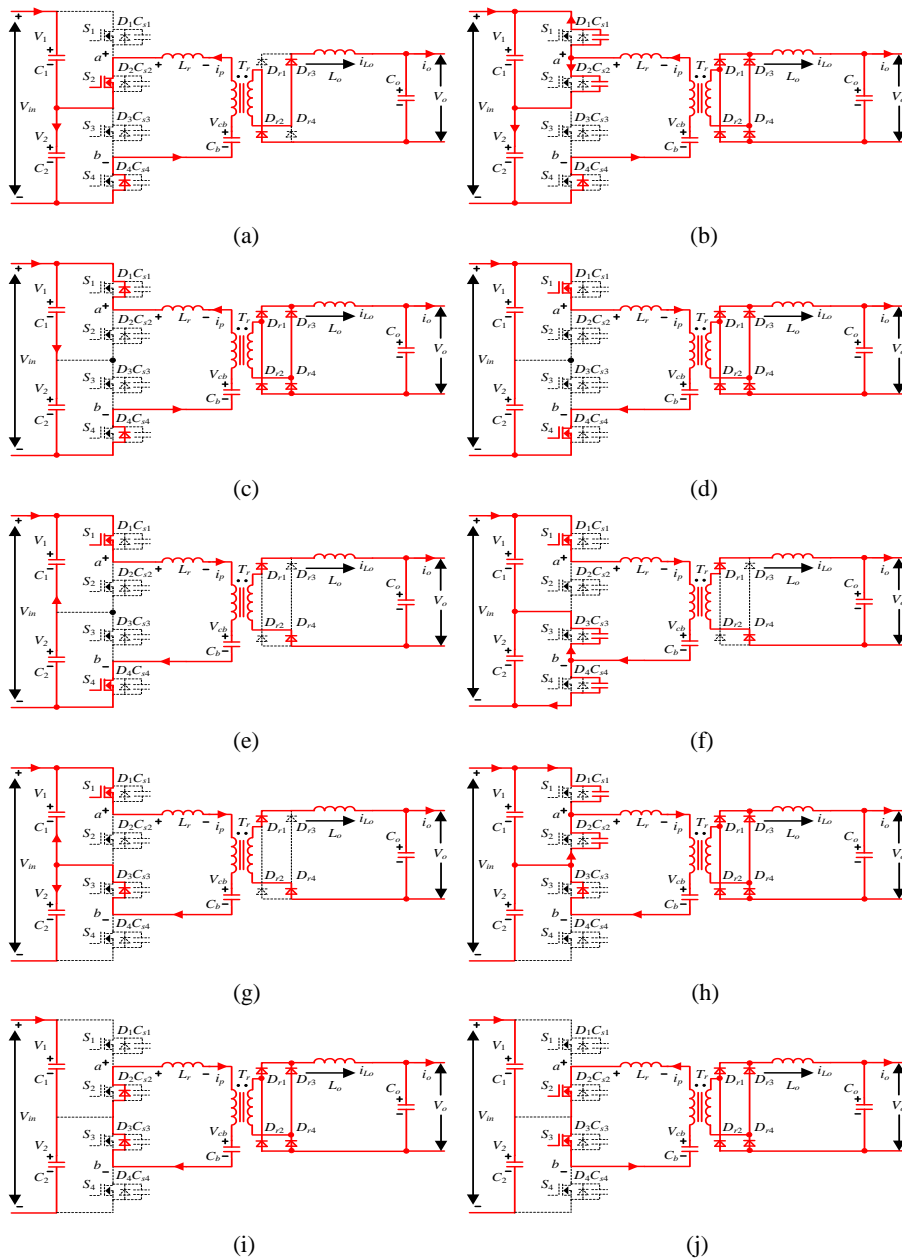


Figure 3-2 Currents on power devices under proposed PSM strategy.

Figure 3-3 presents equivalent circuits to explain working process.



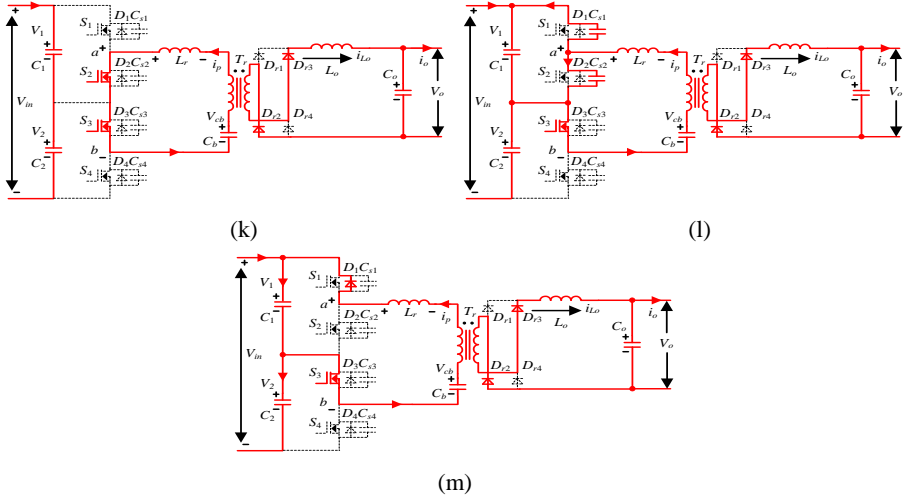


Figure 3-3 Equivalent circuits [102]. (a) [before  $t_2$ ]. (b) [ $t_2 - t_3$ ]. (c) [ $t_3 - t_5$ ]. (d) [ $t_5 - t_6$ ]. (e) [ $t_6 - t_7$ ]. (f) [ $t_7 - t_8$ ]. (g) [ $t_8 - t_9$ ]. (h) [ $t_9 - t_{10}$ ]. (i) [ $t_{10} - t_{12}$ ]. (j) [ $t_{12} - t_{13}$ ]. (k) [ $t_{13} - t_{14}$ ]. (l) [ $t_{14} - t_{15}$ ]. (m) [ $t_{15} - t_{16}$ ].

As presented in Figure 3-2,  $i_1$ ,  $i_2$ ,  $i_3$ , and  $i_4$  are the same during every two switching time periods. Accordingly, only  $i_1$  is given as

$$i_1 = \begin{cases} -\frac{i_o}{n} + \frac{V_{in}}{2 \cdot L_r} \cdot t & [t_2 - t_6] \\ \frac{i_o}{n} & [t_6 - t_9] \\ -\frac{i_o}{n} & [t_{14} - t_{16}] \\ -\frac{i_o}{n} + \frac{V_{in}}{2 \cdot L_r} \cdot t & [t_{16} - t_{20}] \\ \frac{i_o}{n} & [t_{20} - t_{21}] \end{cases} \quad (3.6)$$

In Figure 3-2, the time intervals [ $t_2 - t_6$ ], [ $t_9 - t_{13}$ ], [ $t_{16} - t_{20}$ ] and [ $t_{23} - t_{27}$ ] can be obtained by

$$t_6 - t_2 = t_{13} - t_9 = t_{20} - t_{16} = t_{27} - t_{23} = \frac{4 \cdot L_r \cdot i_o}{n \cdot V_{in}} \quad (3.7)$$

Based on (3.6) and (3.7), RMS value of  $i_1$ ,  $i_2$ ,  $i_3$ , and  $i_4$  under proposed strategy named  $i_{1\_rms\_p}$ ,  $i_{2\_rms\_p}$ ,  $i_{3\_rms\_p}$ , and  $i_{4\_rms\_p}$  are

$$i_{1\_rms\_p} = i_{2\_rms\_p} = i_{3\_rms\_p} = i_{4\_rms\_p} = \sqrt{\frac{i_o^2}{2 \cdot n^2} - \frac{8 \cdot L_r \cdot i_o^3}{3 \cdot n^3 \cdot V_{in} \cdot T_s}} \quad (3.8)$$

*Table 3-1 Calculation formulas about RMS value of  $i_1 \sim i_4$*

Control Strategy	RMS Value	Theoretical Calculation Formula
Conventional modulation Strategies	$i_{1\_rms\_c}$ $i_{3\_rms\_c}$	$\sqrt{\frac{i_o^2}{n^2} \cdot d_1 - \frac{8 \cdot L_r \cdot i_o^3}{3 \cdot n^3 \cdot V_{in} \cdot T_s}}$
	$i_{2\_rms\_c}$ $i_{4\_rms\_c}$	$\sqrt{\frac{i_o^2}{n^2} \cdot d_2 - \frac{8 \cdot L_r \cdot i_o^3}{3 \cdot n^3 \cdot V_{in} \cdot T_s}}$
Proposed modulation Strategy	$i_{1\_rms\_p}$ $i_{2\_rms\_p}$ $i_{3\_rms\_p}$ $i_{4\_rms\_p}$	$\sqrt{\frac{i_o^2}{2 \cdot n^2} - \frac{8 \cdot L_r \cdot i_o^3}{3 \cdot n^3 \cdot V_{in} \cdot T_s}}$

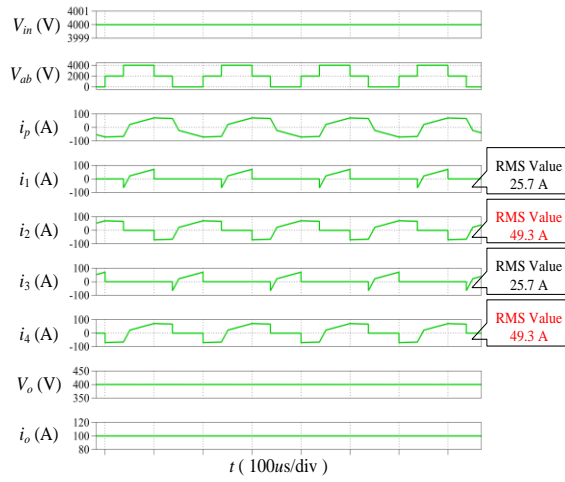
### 3.3. SIMULATION AND EXPERIMENTAL VERIFICATION

#### A. Simulation verification

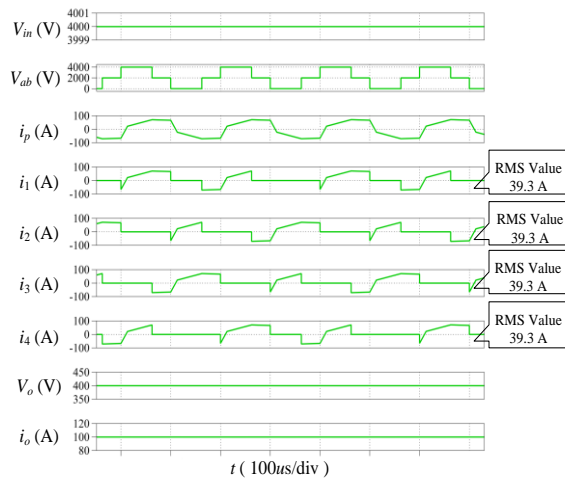
Table 3-2 presents parameters of built simulation model. Figure 3-4 shows simulation results, in which 1) current pairs ( $i_{1\_rms\_c}$ ,  $i_{3\_rms\_c}$ ) and ( $i_{2\_rms\_c}$ ,  $i_{4\_rms\_c}$ ) are 25.7 A are 49.3 A respectively; however, 2)  $i_{1\_rms\_p}$ ,  $i_{2\_rms\_p}$ ,  $i_{3\_rms\_p}$ , and  $i_{4\_rms\_p}$  are all 39.3 A.

*Table 3-2 Parameters of established simulation model*

Description	Parameter
Input voltage $V_{in}$ (kV)	4
Output voltage $V_o$ (V)	400
Output current $i_o$ (A)	100
Turns Ratio of Transformer $T_r$	15 : 7
Leakage Inductance $L_r$ ( $\mu$ H)	300
Output Filter Capacitor $C_o$ ( $\mu$ F)	4700
Output Filter Inductor $L_o$ ( $\mu$ H)	1500
Input Capacitors $C_1$ and $C_2$ ( $\mu$ F)	4700
DC-blocking Capacitor $C_b$ ( $\mu$ F)	100
Switching Frequency (kHz)	5
Dead Time ( $\mu$ s)	1



(a)



(b)

Figure 3-4 Simulation results ( $V_{in} = 4 \text{ kV}$ ,  $V_o = 400 \text{ V}$ ,  $i_o = 100 \text{ A}$ ). (a) Asymmetrical modulation strategy. (b) Proposed strategy.

## B. Experimental verification

Table 3-3 presents parameters of established prototype. The hardware of established prototype and control block have already been presented in Figures 2-7 and 2-8 respectively, which are not repeated here.

Tabel 3-3 Parameters of established prototype

Description	Parameter
Power Switches $S_1 - S_4$	SPW47N60C3
Rectifier Diodes $D_{r1} - D_{r4}$	MBR40250TG
Turns Ratio of Transformer $T_r$	25 : 8
Leakage Inductance $L_r$ of $T_r$ ( $\mu\text{H}$ )	20.7
Output Filter Capacitor $C_o$ ( $\mu\text{F}$ )	470
Output Filter Inductor $L_o$ ( $\mu\text{H}$ )	140
Input Capacitors $C_1$ and $C_2$ ( $\mu\text{F}$ )	11
DC-blocking Capacitor $C_b$ ( $\mu\text{F}$ )	12
Switching Frequency (kHz)	50
Dead Time (ns)	400

Figures 3-5 ~ 3-7 show the experimental results. In Figures 3-6(a) and 3-7(a),  $i_{1\_rms\_c}$ ,  $i_{2\_rms\_c}$ ,  $i_{3\_rms\_c}$ , and  $i_{4\_rms\_c}$  are 2.05 A, 3.10 A, 2.08 A, and 3.12 A under 500 W and 3.86 A, 5.63 A, 3.79 A, and 5.59 A under 1 kW. After utilizing the proposed PSM strategy,  $i_{1\_rms\_p}$ ,  $i_{2\_rms\_p}$ ,  $i_{3\_rms\_p}$ , and  $i_{4\_rms\_p}$  are 2.57 A, 2.61 A, 2.58 A, and 2.64 A under 500 W and 4.75 A, 4.76 A, 4.68 A, and 4.73 A under 1 kW as shown in Figures 3-6(b) and 3-7(b).

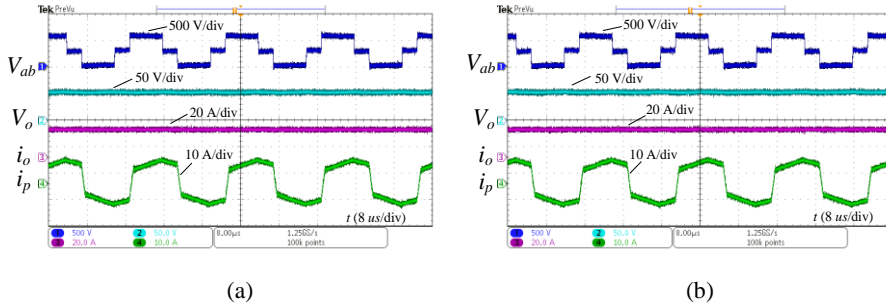
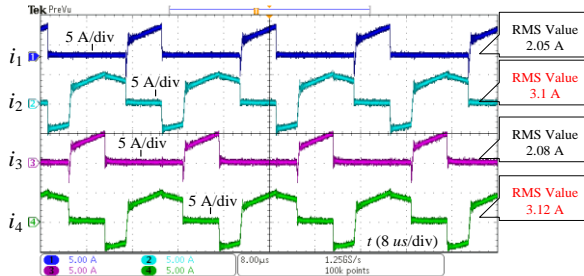
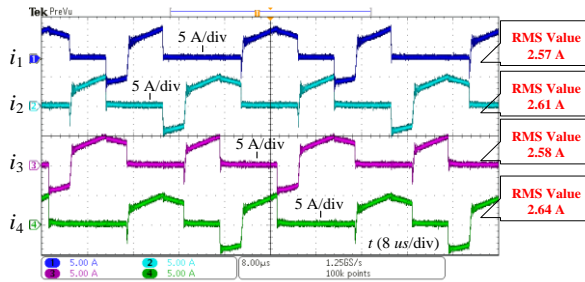


Figure 3-5 Experimental results of  $V_{ab}$ ,  $V_o$ ,  $i_o$ , and  $i_p$  ( $V_{in} = 550$  V,  $V_o = 50$  V,  $P_o = 1$  kW) [102]. (a) Asymmetrical modulation strategy. (b) Proposed strategy.

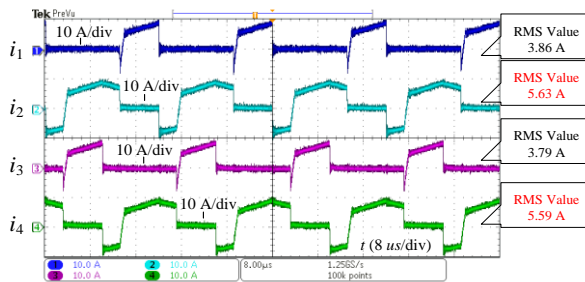


(a)

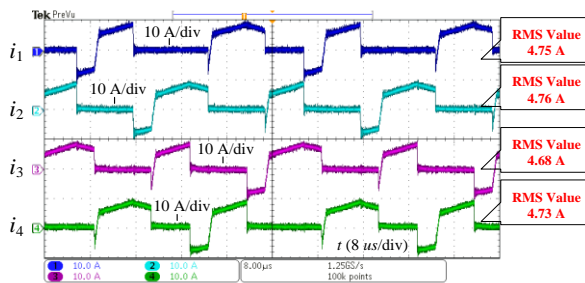


(b)

Figure 3-6 Experimental results of  $i_1$ ,  $i_2$ ,  $i_3$ , and  $i_4$  ( $V_{in} = 550$  V,  $V_o = 50$  V,  $P_o = 500$  W) [102]. (a) Asymmetrical modulation strategy. (b) Proposed strategy.



(a)



(b)

Figure 3-7 Experimental results of  $i_1$ ,  $i_2$ ,  $i_3$ , and  $i_4$  ( $V_{in} = 550$  V,  $V_o = 50$  V,  $P_o = 1$  kW) [102]. (a) Asymmetrical modulation strategy. (b) Proposed strategy.

Figure 3-8 presents experimental RMS value of  $i_1$ ,  $i_2$ ,  $i_3$ , and  $i_4$ . The experimental results in Figure 3-8 can verify that proposed strategy would effectively get rid of power devices' current imbalance.

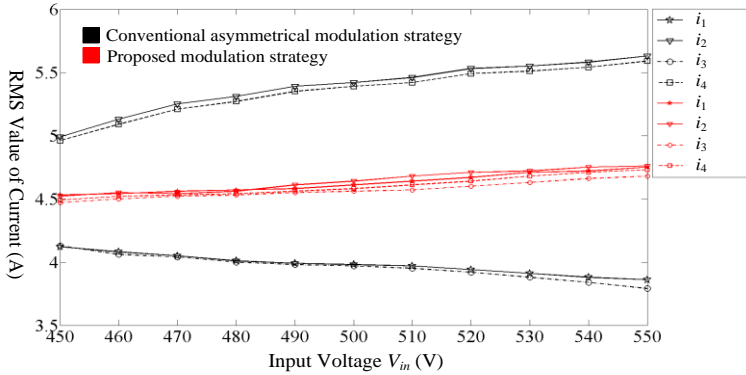


Figure 3-8 Experimental RMS value of  $i_1$ ,  $i_2$ ,  $i_3$ , and  $i_4$  ( $V_o = 50$  V,  $P_o = 1$  kW).

Figure 3-9 shows comparison results about power devices' thermal stresses between conventional and proposed strategy. From Figure 3-9, it can be observed that: 1) temperature of ( $S_2$ ,  $D_2$ ) and ( $S_4$ ,  $D_4$ ) are higher than that of ( $S_1$ ,  $D_1$ ) and ( $S_3$ ,  $D_3$ ) under conventional strategy; and 2) temperature of ( $S_1$ ,  $D_1$ ), ( $S_2$ ,  $D_2$ ), ( $S_3$ ,  $D_3$ ), and ( $S_4$ ,  $D_4$ ) are almost same by utilizing proposed strategy; 3) primary power devices' maximum temperature can be reduced from 34.5 C to 29.3 C due to proposed strategy.

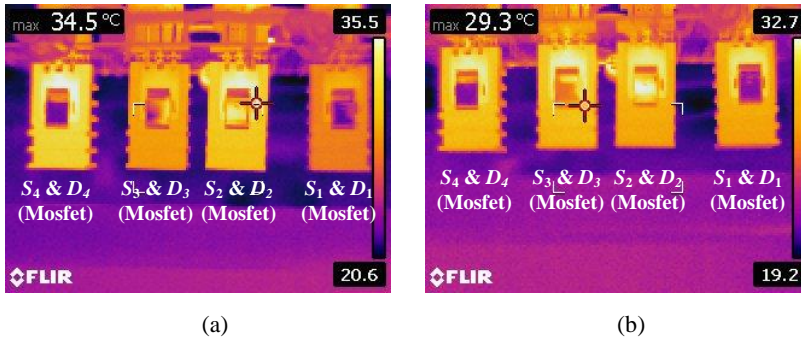


Figure 3-9 Comparison results about power devices' thermal stresses ( $V_{in} = 550$  V,  $V_o = 50$  V,  $P_o = 1$  kW) [102]. (a) Asymmetrical modulation strategy. (b) Proposed strategy.

### 3.4. SUMMARY

In this chapter, the proposed PSM strategy is utilized for several TL IDCs with asymmetrical modulation strategy to balance power devices' currents, which would thus effectively balance power devices' power loss and thermal stress. Simulation results and experimental results both validate proposed strategy. The paper related to this chapter is J3.



# CHAPTER 4. IMPROVING TRANSFORMER PERFORMANCE

This chapter aims at improving transformer performance of FB diode-clamped TL isolated DC/DC converter. Therefore, a new DPS control strategy is proposed to decrease  $dv/dt$  on transformer.

## 4.1. VOLTAGE CHANGES ON TRANSFORMER UNDER CONVENTIONAL CONTROL STRATEGY

Figure 4-1 shows structure of FB diode-clamped TL isolated DC/DC converter and working principle under conventional control strategies. In Figure 4-1,  $V_{in}$  is input voltage;  $C_{i1}$  and  $C_{i2}$  are input capacitors to split  $V_{in}$  into  $V_1$  and  $V_2$ ;  $S_1$ - $S_8$  and  $D_1$ - $D_8$  are power switches and diodes;  $C_1$  -  $C_8$  are junction capacitors of  $S_1$  -  $S_8$ ;  $C_{s1}$  and  $C_{s2}$  are two flying capacitors;  $D_9$ - $D_{12}$  are clamped diodes;  $T_r$  is the isolated transformer;  $L_r$  is leakage inductance of  $T_r$ ;  $D_{r1}$ - $D_{r4}$  are four rectifier diodes;  $L_o$  and  $C_o$  are filter inductor and capacitor. Additionally,  $V_{ab}$  is voltage from point  $a$  to  $b$ ;  $i_p$  is primary current of  $T_r$ ;  $i_{Lo}$  is current on  $L_o$ ;  $V_o$  and  $I_o$  are the output voltage and current; and  $n$  is turns ratio in  $T_r$ . Figures 4-2 and 4-3 presents conventional control strategies named chopping plus phase shift (CPS) [97] and DPS control [98] for FB diode-clamped TL isolated DC/DC converter. From Figures 4-2 and 4-3, it can be seen that maximum voltage change in these conventional control strategies are both from 0 to  $V_{in}$  or 0 to  $-V_{in}$  as marked by red color, which would thus cause high  $dv/dt$ .

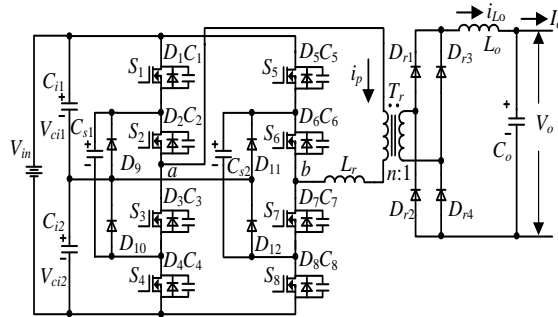


Figure 4-1 Circuit structure.

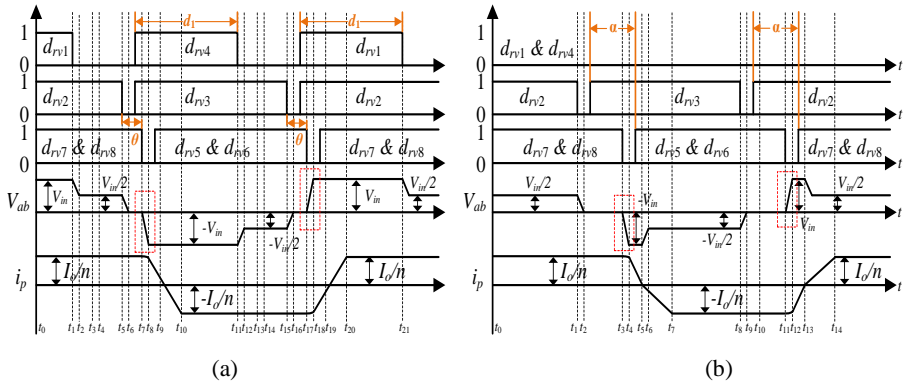


Figure 4-2 Chopping plus phase shift (CPS) control [97]. (a) Three-level mode. (b) Two-level mode.

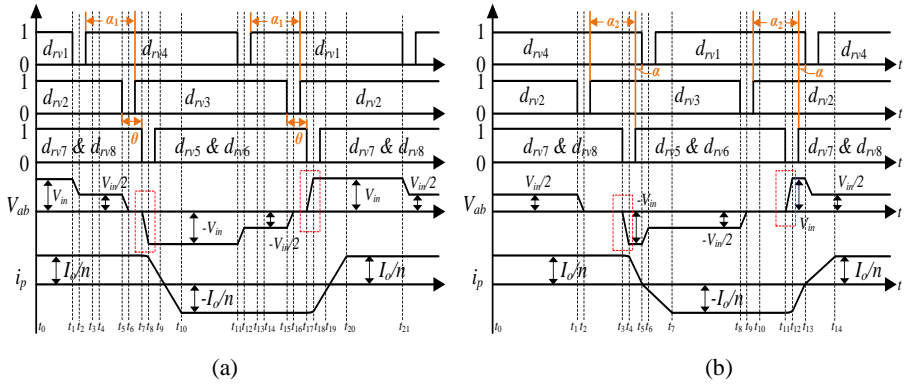


Figure 4-3 Double phase-shift (DPS) control [98]. (a) Three-level mode. (b) Two-level mode.

## 4.2. PROPOSED DPS CONTROL STRATEGY

Figure 4-4 presents working principle of proposed new DPS control strategy. In Figure 4-4,  $d_{rv1}$ - $d_{rv8}$  are driving signals for  $S_1$ - $S_8$ ;  $\alpha_1$  and  $\alpha_2$  are two time delays.

Some assumptions are used to simplify following analysis: 1)  $S_1 - S_8$  have same parasitic capacitors; 2)  $C_{i1}$  and  $C_{i2}$  are regarded to be constant voltage sources ( $V_{in}/2$ ); 3)  $C_{s1}$  and  $C_{s2}$  are regarded to be constant voltage sources ( $V_{in}/2$ ); and 4)  $L_o$  is regarded to be a constant current source.

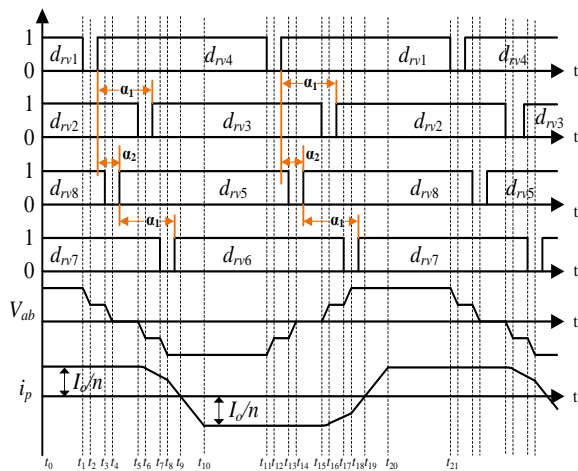
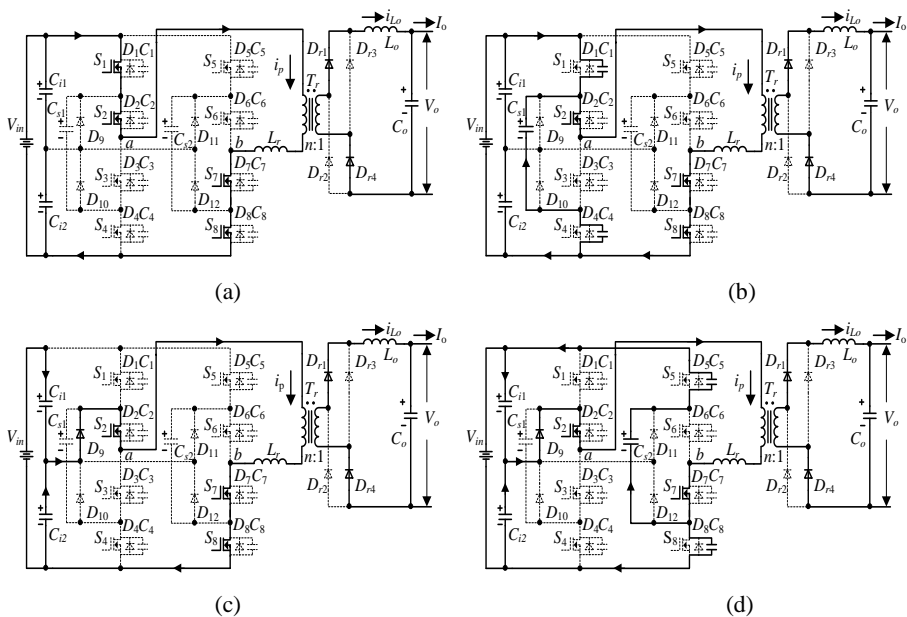


Figure 4-4 Proposed strategy (Three level mode).

Figure 4-5 presents equivalent circuits to explain working process.



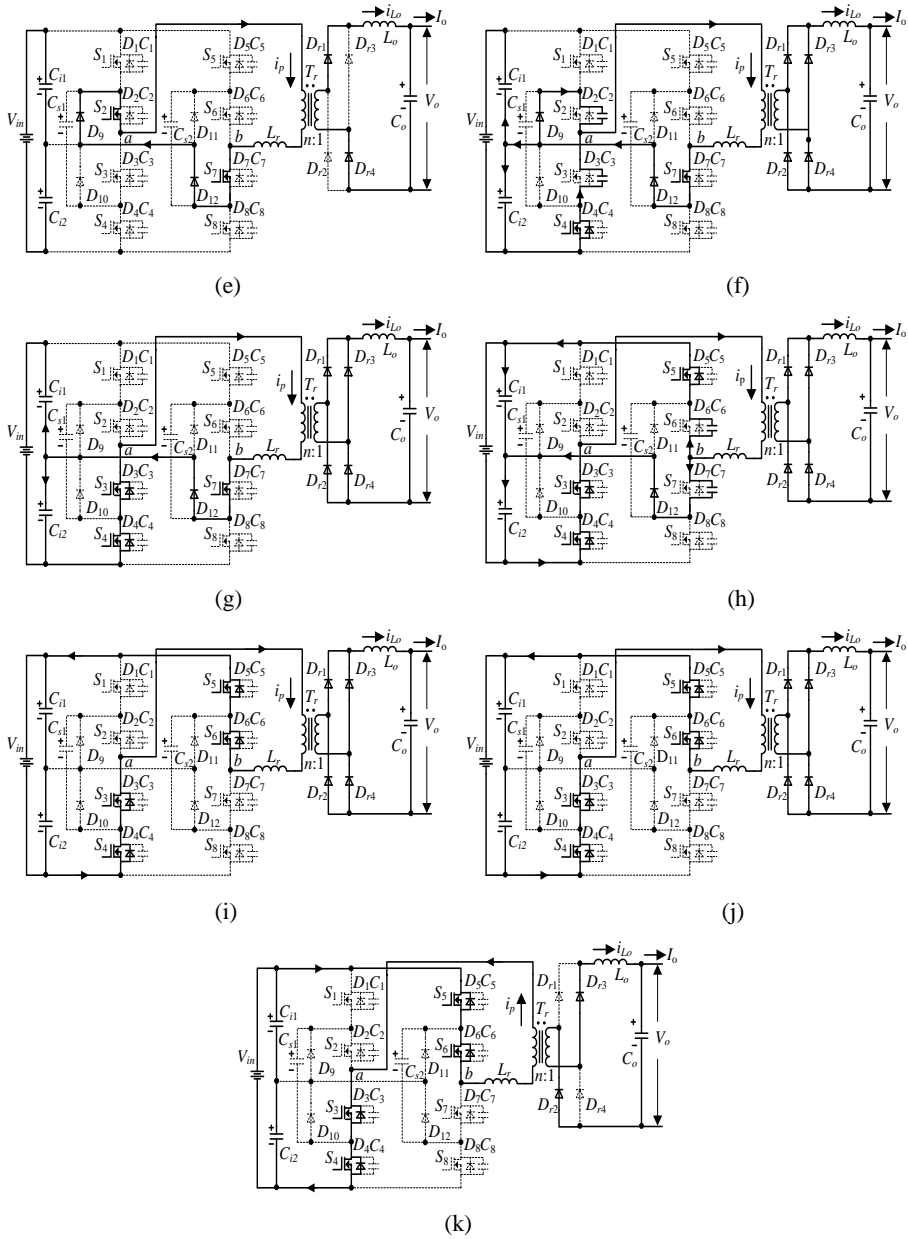


Figure 4-5 Equivalent circuits [103]. (a)  $[t_0-t_1]$ . (b)  $[t_1-t_2]$ . (c)  $[t_2-t_3]$ . (d)  $[t_3-t_4]$ . (e)  $[t_4-t_5]$ . (f)  $[t_5-t_6]$ . (g)  $[t_6-t_7]$ . (h)  $[t_7-t_8]$ . (i)  $[t_8-t_9]$ . (j)  $[t_9-t_{10}]$ . (k)  $[t_{10}-t_{11}]$ .

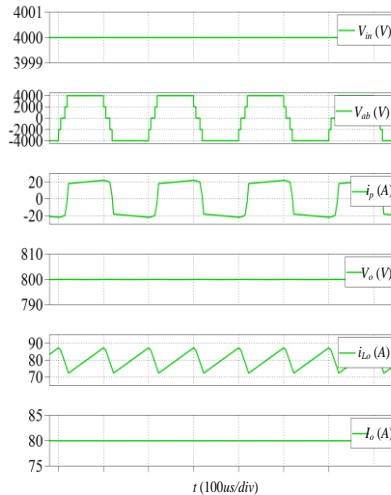
### 4.3. SIMULATION VERIFICATION

Table 4-1 presents parameters of built simulation model. In simulations,  $\alpha_2$  is  $5\mu s$ ;  $V_o$  is controlled by adjusting  $\alpha_1$ .

*Tabel 4-1 Parameters of established simulation model*

Component	Description
Turns Ratio of the Transformer $T_r$ ( $n : 1$ )	4 : 1
Input Capacitors $C_1$ and $C_2$ ( $\mu F$ )	4700
Output Filter Inductor $L_o$ ( $\mu H$ )	1000
Output Filter Capacitor $C_o$ ( $\mu F$ )	4700
Input Voltage $V_{in}$ (kV)	4
Output Voltage $V_o$ (V)	800
$\alpha_2$ ( $\mu s$ )	5
Output Power (kW)	64
Switching Frequency (kHz)	5

Figures 4-6 and 4-7 show simulation results. From comparison results between conventional strategies [97], [98] and proposed strategy, it can be seen that  $dv/dt$  on  $V_{ab}$  is decreased after using the proposed strategy. Therefore, voltage stress of transformer would be decreased.



*Figure 4-6 Simulation results under proposed DPS strategy.*

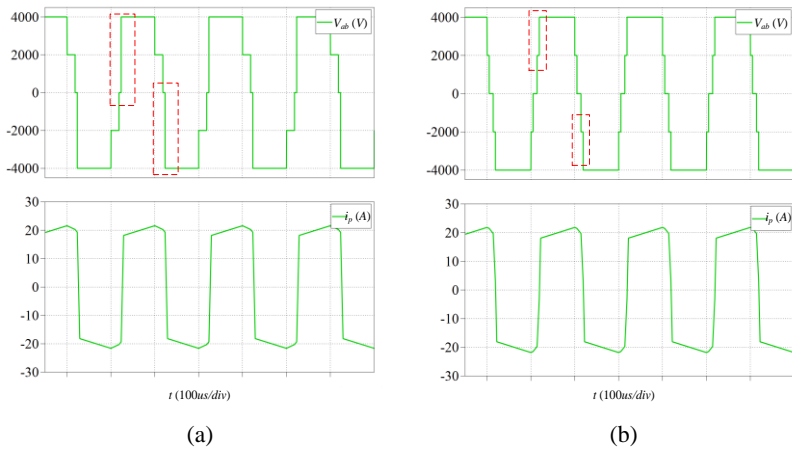


Figure 4-7 Comparison results. (a) Conventional strategies. (b) Proposed strategy.

#### 4.4. SUMMARY

This chapter proposes a new DPS control strategy for FB diode-clamped TL isolated DC/DC converter to decrease voltage changes on transformer, which would decrease the  $dv/dt$  and voltage stress on transformer. Simulation results validate the proposed strategy. The paper related to this chapter is C1.

## CHAPTER 5. CONCLUSIONS AND FUTURE WORKS

This project proposes new topology and modulation strategies to improve reliability performances of input capacitors, power devices, and transformer in TL-IDCs.

### 1) Improving input capacitor performances

There exists an issue of input capacitor current imbalance in FS-HBTL isolated DC/DC converter when utilizing conventional strategy, which would lead input capacitors' thermal stress and lifetime imbalance. Therefore, this project proposed a ZVS strategy including a PSM strategy to balance input capacitors' currents, which would thus balance input capacitors' thermal stress and lifetime. Additionally, this project proposes IPOP TL IDCs to balance and decrease input capacitors' currents, which would thus reduce input capacitors' size and prolong input capacitors' lifetime. Simulation and experimental results both validate proposed control strategy and topology.

### 2) Improving power device performance

The power devices' current imbalance issue exists in kinds of TL-IDCs with asymmetrical modulation. Accordingly, the proposed PSM strategy are utilized for these TL-IDCs to balance power devices' currents, which would thus increase converter's reliability through balancing power devices' power loss and thermal stress. Simulation results and experimental results both validate proposed strategy.

### 3) Improving transformer performance

This project proposes a new DPS control strategy for FB diode-clamped TL isolated DC/DC converter. Comparing with conventional control strategies,  $dv/dt$  and voltage stress on transformer would be reduced by proposed control strategy, which would thus increase converter's reliability. Simulation results validate proposed strategy.

There are many works can be further proceeded in future based on this thesis. The future works include but are not limited to followings:

- Investigate performances (currents on power devices, input capacitors, and flying capacitors) about FB diode-clamped TL IDCs;
- Investigate performances (currents on power devices, input capacitors, and flying capacitors) about T-type TL IDCs;

- Expand proposed PSM strategy to other hybrid TL-IDCs or other types of converters.



# LITERATURE LIST

- [1] H. Farhangi, "The path of the smart grid," *IEEE Power Energy Mag.*, vol. 8, no. 1, pp. 18–28, Jan./Feb. 2010.
- [2] H. Kakigano, Y. Miura, T. Ise, and R. Uchida, "DC micro-grid for super high quality distribution—System configuration and control of distributed generations and energy storage devices," in *Proc. IEEE IPEMC*, 2004, pp. 1–7.
- [3] J. M. Guerrero, J. C. Vasquez, J. Matas, L. G. De Vicuna, and M. Castilla, "Hierarchical control of droop-controlled ac and dc microgrids- A general approach toward standardization," *IEEE Trans. Ind. Electron.*, vol. 58, no. 1, pp. 158–172, Jan. 2011.
- [4] H. Mohsenian-Rad and A. Davoudi, "Towards building an optimal demand response framework for DC distribution networks," *IEEE Trans. Smart Grid.*, vol. 5, no. 5, pp. 2626–2634, Sep. 2014.
- [5] G. F. Reed, B. M. Grainger, A. R. Sparacino, and M. Zhi-Hong, "Ship to grid: Medium-voltage DC concepts in theory and practice," *IEEE Power Energy Mag.*, vol. 10, no. 6, pp. 70–79, Nov. 2012.
- [6] F. Chen, R. Burgos, D. Boroyevich, and W. Zhang, "A nonlinear droop method to improve voltage regulation and load sharing in DC systems," in *Proc. IEEE ICDCM*, 2015, pp. 45–50.
- [7] N. Flourentzou, V. G. Agelidis, and G. D. Demetriades, "VSC-based HVDC power transmission systems: An overview," *IEEE Trans. Power Electron.*, vol. 24, no. 3, pp. 592–602, Mar. 2009.
- [8] F. Chen, W. Zhang, R. Burgos, and D. Boroyevich, "Droop voltage range design in DC micro-grids considering cable resistance," in *Proc. IEEE ECCE*, 2014, pp. 770–777.
- [9] J. Rocabert, A. Luna, F. Blaabjerg, and P. Rodriguez, "Control of power converters in AC microgrids," *IEEE Trans. Power Electron.*, vol. 27, no. 11, pp. 4734–4749, Nov. 2012.
- [10] F. Chen, R. Burgos, D. Boroyevich and X. Zhang, "Low-frequency common-mode voltage control for systems interconnected with power converters," *IEEE Trans. Ind. Electron.*, vol. 64, no. 1, pp. 873–882, Jan. 2017.
- [11] F. Blaabjerg, R. Teodorescu, M. Liserre, and A. V. Timbus, "Overview of control and grid synchronization for distributed power generation systems," *IEEE Trans. Ind. Electron.*, vol. 53, no. 5, pp. 1398–1409, Oct. 2006.
- [12] S. Anand and B. G. Fernandes, "Optimal voltage level for DC microgrids," in *Proc. IEEE Conf. Ind. Electron.*, 2010, pp. 3034–3039.
- [13] D. Salomonsson, L. Soder, and A. Sannino, "An adaptive control system for a DC microgrid for data centers," *IEEE Trans. Ind. Appl.*, vol. 44, no. 6, pp. 1910–1917, Nov./Dec. 2008.
- [14] W. Chen, A. Q. Huang, C. Li, G. Wang, and W. Gu, "Analysis and comparison of medium voltage high power DC/DC converters for offshore wind energy systems," *IEEE Trans. Power Electron.*, vol. 28, no. 4, pp. 2014–2023, Apr. 2013.
- [15] L. Max and S. Lundberg, "System efficiency of a DC/DC converter-based wind farm," *Wind Energy*, pp. 109–120, 2008.

- [16] D. Jovcic, "Bidirectional, high-power DC transformer," *IEEE Trans. Power Del.*, vol. 24, no. 4, pp. 2276–2283, Oct. 2009.
- [17] W. H. Li and X. N. He, "Review of non-isolated high step-up DC/DC converters in photovoltaic grid-connected applications," *IEEE Trans. Ind. Electron.*, vol. 58, no. 4, pp. 1239–1250, Apr. 2011.
- [18] L. W. Zhou, B. X. Zhu, Q. M. Luo, and S. Chen, "Interleaved non-isolated high step-up DC/DC converter based on the diode–capacitor multiplier," *IET Power Electron.*, vol. 7, no. 2, pp. 390–397, Feb. 2014.
- [19] C. T. Pan, C. F. Chuang, and C. C. Chu, "A novel transformerless adaptable voltage quadrupler DC converter with low switch voltage stress," *IEEE Trans. Power Electron.*, vol. 29, no. 9, pp. 4787–4796, Sep. 2014.
- [20] B. Axelrod, Y. Berkovich, and A. Ioinovici, "Switched-capacitor/switched-inductor structures for getting transformerless hybrid DC–DC PWM converters," *IEEE Trans. Circuits Syst. I, Reg. Papers.*, vol. 55, no. 2, pp. 687–696, Mar. 2008.
- [21] Y. Tang, T. Wang, and Y. H. He, "A switched-capacitor-based active network converter with high voltage gain," *IEEE Trans. Power Electron.*, vol. 29, no. 6, pp. 2959–2968, Jun. 2014.
- [22] L. S. Yang, T. J. Liang, and J. F. Chen, "Transformerless DC–DC converters with high step-up voltage gain," *IEEE Trans. Ind. Electron.*, vol. 56, no. 8, pp. 3144–3152, Aug. 2009.
- [23] X. Wu, J. Zhang, X. Ye, and Z. Qian, "Analysis and derivations for a family ZVS converter based on a new active clamp ZVS cell," *IEEE Trans. Ind. Electron.*, vol. 55, no. 2, pp. 773–781, Feb. 2008.
- [24] T. F. Wu, Y. S. Lai, J. C. Hung, and Y. M. Chen, "Boost converter with coupled inductors and buck–boost type of active clamp," *IEEE Trans. Ind. Electron.*, vol. 55, no. 1, pp. 154–162, Jan. 2008.
- [25] T. F. Wu, Y. S. Lai, J. C. Hung, and Y. M. Chen, "An improved boost converter with coupled inductors and buck–boost type of active clamp," in *Proc. Conf. Rec. IEEE IAS Annu. Meeting*, 2005, pp. 639–644.
- [26] T. Soong and P. Lehn, "A transformerless high boost dc-dc converter for use in medium/high voltage applications," in *Proc. IEEE 38th Annu. Conf. Ind. Electron. Soc.*, 2012, pp. 174–179.
- [27] L. Zhu, "A novel soft-commutating isolated boost full-bridge ZVS-PWM DC-DC converter for bidirectional high power applications," *IEEE Trans. Power Electron.*, vol. 21, no. 2, pp. 422–429, Mar. 2006.
- [28] D. Vinnikov and I. Roasto, "Quasi-Z-source-based isolated DC/DC converters for distributed power generation," *IEEE Trans. Ind. Electron.*, vol. 58, no. 1, pp. 192–201, Jan. 2011.

- [29] Y. Li, X. Ruan, D. Yang, F. Liu, and C. K. Tse, "Synthesis of multiple input DC/DC converters," *IEEE Trans. Power Electron.*, vol. 25, no. 9, pp. 2372–2385, Sep. 2010.
- [30] X. Li and A. Bhat, "Analysis and design of high-frequency isolated dual bridge series resonant DC/DC converter," *IEEE Trans. Power Electron.*, vol. 25, no. 4, pp. 850–862, Apr. 2010.
- [31] Z. Qian, O. Abdel-Rahman, and I. Batarseh, "An integrated four-port dc/dc converter for renewable energy applications," *IEEE Trans. Power Electron.*, vol. 25, no. 7, pp. 1877–1887, Jul. 2010.
- [32] C. Liu, A. Johnson, and J. S. Lai, "A novel three-phase high-power soft switched DC/DC converter for low-voltage fuel cell applications," *IEEE Trans. Power Electron.*, vol. 41, no. 6, pp. 1691–1697, Nov./Dec. 2005.
- [33] F. Krismer, J. Biela, and J. W. Kolar, "A comparative evaluation of isolated bi-directional DC/DC converters with wide input and output voltage range," in *Proc. 40th Ind. Appl. Soc. Annu. Meeting Conf. Rec.*, 2005, pp. 599–606.
- [34] I.-O. Lee and G.-W. Moon, "Analysis and design of a three-level LLC series resonant converter for high- and wide-input-voltage applications," *IEEE Trans. Power Electron.*, vol. 27, no. 6, pp. 2966–2979, Apr. 2012.
- [35] J.-Y. Lee, Y.-S. Jeong, and B.-M. Han, "An isolated DC/DC converter using high-frequency unregulated LLC resonant converter for fuel cell applications," *IEEE Trans. Ind. Electron.*, vol. 58, no. 7, pp. 2926–2934, Jul. 2011.
- [36] W. Li and X. He, "A family of isolated interleaved boost and buck converters with winding-cross-coupled inductors," *IEEE Trans. Power Electron.*, vol. 23, no. 6, pp. 3164–3173, Nov. 2008.
- [37] Z. Qian, O. A. Rahman, H. A. Atrash, and I. Batarseh, "Modeling and control of three-port DC/DC converter interface for satellite applications," *IEEE Trans. Power Electron.*, vol. 25, no. 3, pp. 637–649, Mar. 2010.
- [38] D. Liu, F. Deng, and Z. Chen, "Five-level active-neutral-point-clamped DC/DC converter for medium voltage DC grids," *IEEE Trans. Power Electron.*, vol. 32, no. 5, pp. 3402–3412, May. 2017.
- [39] U. Prasanna and A. Rathore, "Extended range ZVS active-clamped current-fed full-bridge isolated DC/DC converter for fuel cell applications: Analysis, design and experimental results," *IEEE Trans. Ind. Electron.*, vol. 60, no. 7, pp. 2661–2672, Jul. 2013.
- [40] M. Pahlevaninezhad, P. Das, J. Drobniak, P. Jain, and A. Bakhshai, "A novel ZVZCS full-bridge DC/DC converter used for electric vehicles," *IEEE Trans. Power Electron.*, vol. 27, no. 6, pp. 2752–2769, Jun. 2012.
- [41] Y. Jang, M. M. Jovanovic, and Y.-M. Chang, "A new ZVS-PWM full bridge converter," *IEEE Trans. Power Electron.*, vol. 18, no. 5, pp. 1122–1129, Sep. 2003.

- [42] A. Averbeg and A. Mertens, "Analysis of a voltage-fed full bridge DC-DC converter in fuel cell systems," in *Proc. IEEE Power Electron. Spec. Conf., (PESC)*, 2007, pp. 286–292.
- [43] J. A. Sabate, V. Vlatkovic, R. B. Ridley, and F. C. Lee, "High-voltage, high power, ZVS, full-bridge PWM converter employing an active snubber," in *Proc. 6th Annu. Appl. Power Electron. Conf. Expo.*, 1991, pp. 158–163.
- [44] J. Kim, H.-S. Song, and K. Nam, "Asymmetric duty control of a dual-half bridge DC/DC converter for single-phase distributed generators," *IEEE Trans. Power Electron.*, vol. 26, no. 3, pp. 973–982, Mar. 2011.
- [45] H. Xu, L. Kong, and X. Wen, "Fuel cell power system and high power DC-DC converter," *IEEE Trans. Power Electron.*, vol. 19, no. 5, pp. 1250–1255, Sept. 2004.
- [46] D. Vinnikov, T. Jalakas, and M. Egorov, "Feasibility study of half- and full-bridge isolated DC/DC converters in high-voltage high-power applications," in *Proc. 13th Power Electron. Motion Control Conf.*, 2008, pp.1257–1262.
- [47] G. Ortiz, J. Biela, D. Bortis, and J. Kolar, "1 Megawatt, 20 kHz, isolated, bidirectional 12 kV to 1.2 kV DC-DC converter for renewable energy applications," in *Proc. Int. Power Electron. Conf.*, 2010, pp. 3212–3219.
- [48] F. Blaabjerg, F. Iov, Z. Chen, and K. Ma, "Power electronics and controls for wind turbine systems," in *Proc. IEEE Int. Energy Conf. Exhib.*, 2010, pp. 333–344.
- [49] N. Mohan, T. M. Undeland, and W. P. Robbins, "Power Electronics: Converters, Applications, and Design," 3rd ed. New York, NY, USA: Wiley, 2003.
- [50] S. Kenzelmann, A. Rufer, D. Dujic, F. Canales, and Y. R. de Novaes, "Isolated DC/DC structure based on modular multilevel converter," *IEEE Trans. Power Electron.*, vol. 30, no. 1, pp. 89–98, Jan. 2015.
- [51] S. Kenzelmann, A. Rufer, M. Vasiladiotis, D. Dujic, F. Canales, and Y. R. de Novaes, "A versatile DC-DC converter for energy collection and distribution using the modular multilevel converter," in *Proc. 14th Eur. Conf. Power Electron. Appl.*, 2011, pp. 1–10.
- [52] J. A. Ferreira, "The multilevel modular DC converter," *IEEE Trans. Power Electron.*, vol. 28, no. 10, pp. 4460–4465, Oct. 2013.
- [53] R. Mo, R. Li, and H. Li, "Isolated modular multilevel (IMM) DC/DC converter with energy storage and active filter function for shipboard MVDC system applications," in *Proc. IEEE Electric Ship Technol. Symp.*, 2015, pp. 113–117.
- [54] Wang, Z.; Wang, T.; Zhang, J., "Three phase modular multilevel DC/DC converter for power electronic transformer application", in *Proc. Energy Conversion Congress and Exposition (ECCE)*, 2015, pp. 6277–6284.
- [55] S. Du, B. Wu, K. Tian, D. Xu, and N. Zargari, "A novel medium-voltage modular multilevel DC-DC converter," *IEEE Trans. Ind. Electron.*, vol. 63, no. 12, pp. 7939–7949, Dec. 2016.

- [56] R. Mo, R. Li, and H. Li, "Isolated modular multilevel (IMM) DC/DC converter with energy storage and active filter function for shipboard MVDC system applications," in *Proc. Electric Ship Technology Symposium*, 2015, pp. 113–117.
- [57] Shi Y, Li R, and Li H, "Modular multilevel dual active bridge DC-DC converter with ZVS and fast DC fault recovery for battery energy storage systems," in *Proc. IEEE APEC*, 2016, pp. 1675–1681.
- [58] S. Debnath, J. Qin, B. Bahrani, M. Saadifard, and P. Barbosa, "Operation, control, and applications of the modular multilevel converter: A review," *IEEE Trans. Power Electron.*, vol. 30, no. 1, pp. 37–53, Jan. 2015.
- [59] F. Deng and Z. Chen, "A control method for voltage balancing in modular multilevel converters," *IEEE Trans. Power Electron.*, vol. 29, no. 1, pp. 66–76, Jan. 2014.
- [60] F. Deng and Z. Chen, "Voltage-balancing method for modular multilevel converters switched at grid frequency," *IEEE Trans. Ind. Electron.*, vol. 62, no. 5, pp. 2835–2847, Jan. 2015.
- [61] E. Solas et al., "Modular multilevel converter with different submodule concepts—Part I: Capacitor voltage balancing method," *IEEE Trans. Ind. Electron.*, vol. 60, no. 10, pp. 4525–4535, Oct. 2013.
- [62] J. R. Pinheiro and I. Barbi, "The three-level ZVS PWM converter—a new concept in high-voltage DC-to-DC conversion," in *Proc. IEEE Int. Conf. Ind. Electron. Control Instrum. Autom.*, 1992, pp. 173–178.
- [63] F. Canales, P. Barbosa, M. Burdío, and F. Lee, "A zero-voltage switching three-level DC/DC converter," in *Proc. 22nd Int. Telecommun. Energy Conf.*, 2000, pp. 512–517.
- [64] F. Canales, P. Barbosa, and F. C. Lee, "A zero-voltage and zero-current switching three-level DC/DC converter," *IEEE Trans. Power Electron.*, vol. 17, no. 6, pp. 898–904, Nov. 2002.
- [65] I.-O. Lee and G.-W. Moon, "Analysis and design of a three-level LLC series resonant converter for high- and wide-input voltage applications," *IEEE Trans. Power Electron.*, vol. 27, no. 6, pp. 2966–2979, Jun. 2012.
- [66] W. Li, P. Li, H. Yang, and X. He, "Three level forward-flyback phase shift ZVS converter with integrated series-connected coupled inductors," *IEEE Trans. Power Electron.*, vol. 27, no. 6, pp. 2846–2856, Jun. 2012.
- [67] H. Sheng, F. Wang, and C. Tipton, "A fault detection and protection scheme for three-level dc-dc converters based on monitoring flying capacitor voltage," *IEEE Trans. Power Electron.*, vol. 27, no. 2, pp. 685–697, Feb. 2012.
- [68] T. T. Sun, H. S. H. Chung, and A. Ioinovici, "A high-voltage DC-DC converter with  $V_{in}/3$ —Voltage stress on the primary switches," *IEEE Trans. Power Electron.*, vol. 22, no. 6, pp. 2124–2137, Nov. 2007.

- [69] X. Ruan, Z. Chen, and W. Chen, “Zero-voltage-switching PWM hybrid full-bridge three-level converter,” *IEEE Trans. Power Electron.*, vol. 20, no. 2, pp. 395–404, Mar. 2005.
- [70] Y. Gu, Z. Lu, and Z. Qian, “Three-level LLC series resonant DC/DC converter,” *IEEE Trans. Power Electron.*, vol. 20, no. 4, pp. 781–789, Jul. 2005.
- [71] Y. Shi and X. Yang, “Soft switching PWM cascaded three-level combined DC–DC converters with reduced filter size and wide ZVS load range,” *IEEE Trans. Ind. Electron.*, vol. 30, no. 12, pp. 6604–6616, Dec. 2015.
- [72] Y. Shi, and X. Yang, “Wide-range soft-switching PWM three-level combined DC–DC converter without added primary clamping devices,” *IEEE Trans. Power Electron.*, vol. 29, no. 10, pp. 5157–5171, Oct. 2014.
- [73] J. L. Duarte, J. Lokos, and F. B. M. V. Horck, “Phase-shift-controlled three-level converter with reduced voltage stress featuring ZVS over the full operation range,” *IEEE Trans. Power Electron.*, vol. 28, no. 5, pp. 2140–2150, May 2013.
- [74] Y. Shi and X. Yang, “Zero-voltage switching PWM three-level full-bridge dc–dc converter with wide ZVS load range,” *IEEE Trans. Power Electron.*, vol. 28, no. 10, pp. 4511–4524, Oct. 2013.
- [75] I. Barbi, R. Gules, R. Redl, and N. O. Sokal, “DC/DC converter: Four switches  $V_{pk} = V_{in} / 2$ , capacitive turn-off snubbing, ZV turn-on,” *IEEE Trans. Power Electron.*, vol. 19, no. 4, pp. 918–927, Jul. 2004.
- [76] B.-R. Lin and C.-H. Liu, “ZVS dc-dc converter based on two three-level PWM circuits sharing the same power switches,” *IEEE Trans. Ind. Electron.*, vol. 60, no. 10, pp. 4191–1503, Oct. 2013.
- [77] D. Kim, J. Kim, and G. Moon, “A three-level converter with reduced filter size using two transformers and flying capacitors,” *IEEE Trans. Power Electron.*, vol. 28, no. 1, pp. 2140–2150, Jan. 2013.
- [78] F. Liu, G. Hu, and X. Ruan, “Three-phase three-level DC/DC converter for high input voltage and high-power applications-adopting symmetrical duty cycle control,” *IEEE Trans. Power Electron.*, vol. 29, no. 1, pp. 56–65, Jan. 2014.
- [79] F. Liu, J. Yan, and X. Ruan, “Zero-voltage and zero-current-switching PWM combined three-level DC/DC converter,” *IEEE Trans. Ind. Electron.*, vol. 57, no. 5, pp. 1644–1654, May 2010.
- [80] B. Lin, and S. Chung, “New parallel ZVS converter with less active switches and smaller output inductance,” *IEEE Trans. Power Electron.*, vol. 29, no. 7, pp. 3297–3307, July. 2014.
- [81] W. Li, Q. Luo, Y. Mei, S. Zong, X. He, and C. Xia, “Flying-capacitor based hybrid LLC converters with input voltage auto-balance ability for high voltage applications,” *IEEE Trans. Power Electron.*, vol. 31, no. 3, pp. 1908–1920, Mar. 2016.

- [82] B. Lin and P. Cheng, "New ZVS DC–DC converter with series-connected transformers to balance the output currents," *IEEE Trans. Power Electron.*, vol. 29, no. 1, pp. 246–255, Jan. 2014.
- [83] Z. Guo, D. Sha, and X. Liao, "Hybrid phase-shift-controlled three-level and LLC DC–DC converter with active connection at the secondary side," *IEEE Trans. Power Electron.*, vol. 30, no. 6, pp. 2985–2996, Jun. 2015.
- [84] Z. Guo, D. Sha, and X. Liao, "Hybrid three-level and half-bridge DC-DC converter with reduced circulating loss and output filter inductance," *IEEE Trans. Power Electron.*, vol. 30, no. 12, pp. 6628–6638, Dec. 2015.
- [85] Z. Guo, K. Sun, and D. Sha, "Improved ZVS three-level DC–DC converter with reduced circulating loss," *IEEE Trans. Power Electron.*, vol. 31, no. 9, pp. 6394–6404, Sep. 2016.
- [86] W. Li, S. Zong, F. Liu, H. Yang, X. He, and B. Wu, "Secondary-side phase-shift-controlled ZVS DC/DC converter with wide voltage gain for high input voltage applications," *IEEE Trans. Power Electron.*, vol. 28, no. 11, pp. 5128–5139, Nov. 2013.
- [87] Z. Guo, K. Sun, and L. Li, "Analysis and evaluation of dual half-bridge cascaded three-level DC–DC converter for reducing circulating current loss," *J. Emerging Sel. Topics Power Electron.*, vol. 5, no. 1, pp. 351–362, Mar. 2017.
- [88] X. Ruan, L. Zhou, and Y. Yan, "Soft-switching PWM three-level converters," *IEEE Trans. Power Electron.*, vol. 16, no. 5, pp. 612–622, Sep. 2001.
- [89] S. Yang *et al.*, "An industry-based survey of reliability in power electronic converters," *IEEE Trans. Ind. Appl.*, vol. 47, no. 3, pp. 1441–1451, May/June. 2011.
- [90] H. Wang and F. Blaabjerg, "Reliability of capacitors for DC-link applications in power electronic converters—An overview," *IEEE Trans. Ind. Appl.*, vol. 50, no. 5, pp. 3569–3578, Sep./Oct. 2014.
- [91] X. Yu, K. Jin, and Z. Liu, "Capacitor voltage control strategy for half-bridge three-level DC/DC converter," *IEEE Trans. Power Electron.*, vol. 29, no. 4, pp. 1557–1561, Apr. 2014.
- [92] B. Lin and S. Zhang, "Analysis and implementation of a three-level hybrid dc–dc converter with the balanced capacitor voltages," *IET Power Electronics*, vol. 9, no. 3, pp. 457–465, Mar. 2016.
- [93] W. Li, Q. Jiang, Y. Mei, C. Li, Y. Deng, and X. He, "Modular multilevel DC/DC converters with phase-shift control scheme for high-voltage DC based systems," *IEEE Trans. Power Electron.*, vol. 30, no. 1, pp. 99–107, Jan. 2015.
- [94] J. S. Lai and F. Z. Peng, "Multilevel converters-A new breed of power converters," *IEEE Trans. Ind. Appl.*, vol. 32, no. 3, pp. 509–517, May/June. 1996.

- [95] E. Deschamps and I. Barbi, "A flying-capacitor ZVS PWM 1.5 kW DC-to-DC converter with half of the input voltage across the switches," *IEEE Trans. Power Electron.*, vol. 15, no. 5, pp. 855–860, Sep. 2000.
- [96] E. Deschamps and I. Barbi, "A comparison among three-level ZVS-PWM isolated DC-to-DC converters," in *Proc. 38th Annu. Conf. IEEE Ind. Electron. Soc.*, 1998, pp. 1024–1029.
- [97] Z. Zhang and X. Ruan, "ZVS PWM full-bridge three-level converter," in *Proc. 4th Int. Power Electron. Motion Control Conf.*, 2004, pp. 1085–1090.
- [98] Z. Zhang and X. Ruan, "A novel double phase-shift control scheme for full-bridge three-level converter," in *Proc. 20th Annu. IEEE Appl. Power Electron. Conf. Expos., Mar.*, 2005, pp. 1240–1245.
- [99] F. Deng and Z. Chen, "Control of improved full-bridge three-level DC/DC converter for wind turbines in a DC grid," *IEEE Trans. Power Electron.*, vol. 28, no. 1, pp. 314–324, Jan. 2013.
- [100] D. Liu, F. Deng, Q. Zhang, and Z. Chen, "Zero-voltage switching PWM strategy based capacitor current-balancing control for half-bridge three-level DC/DC converter," *IEEE Trans. Power Electron.*, vol. 33, no. 1, pp. 357–369, Jan. 2018.
- [101] D. Liu, F. Deng, Z. Gong, and Z. Chen, "Input-parallel output-parallel (IPOP) three-level (TL) DC/DC converters with interleaving control strategy for minimizing and balancing capacitor ripple currents," *J. Emerging Sel. Topics Power Electron.*, vol. 5, no. 3, pp. 1122–1132, Sep. 2017.
- [102] D. Liu, F. Deng, Q. Zhang, and Z. Chen, "Periodically swapping modulation (PSM) strategy for three-level (TL) DC/DC converters with balanced switch currents," in *IEEE Trans. Ind. Electron.*, vol. 65, no. 1, pp. 412–423, Jan. 2018.
- [103] D. Liu, F. Deng, Z. Gong, and Z. Chen, "A double phase-shift control strategy for a full-bridge three-level DC/DC converter," in *Proc. 42nd Annual Conference of the IEEE Industrial Electronics Society (IECON)*, 2016, pp. 1202–1207.



ISSN (online): 2446-1636  
ISBN (online): 978-87-7210-141-5

AALBORG UNIVERSITY PRESS